

NNT : 2016SACLS188

THESE DE DOCTORAT
DE
L'UNIVERSITE PARIS-SACLAY
PREPAREE A
L'UNIVERSITE PARIS-SUD

ECOLE DOCTORALE N° 572 : EDOM
Ecole Doctorale Ondes et Matière

Spécialité de doctorat: Milieux dilués et optique fondamentale

Par

M. Viet Tiep PHUNG

Cavity ring-down spectroscopy of astrophysically relevant molecular species,
toward quantitative and high resolution studies
using spectro-temporal properties of high finesse cavities

Thèse présentée et soutenue à Orsay, le 12 juillet 2016 :

Après avis des rapporteurs :

M. Christof JANSSEN (Chargé de recherche, Laboratoire d'Etudes du Rayonnement et de la Matière en Astrophysique et Atmosphères)

M. Marek TULEJ (Professeur, Institut de physique, Université de Bern)

Composition du Jury :

M. Alain SARFATI	Professeur, Laboratoire Aimé Cotton	Président
M. Christof JANSSEN	Chargé de recherche, Laboratoire d'Etudes du Rayonnement et de la Matière en Astrophysique et Atmosphères	Rapporteur
M. Ludovic BIENNIER	Chargé de recherche, Institut de Physique de Rennes	Examineur
M. Stéphane DOUIN	Maître de conférences Institut des Sciences Moléculaires d'Orsay	Co-encadrant
M. Thomas PINO	Directeur de recherche Institut des Sciences Moléculaires d'Orsay	Directeur de thèse

1.2.3. Cavity Ring-Down Spectroscopy Technique

1.2.3.1. Principle of CRDS

The Cavity Ring-Down Spectroscopy Technique is a direct absorption technique. It generally consists in measuring the decay rate of a laser pulse (having the wavelength λ) sent into a rigid optical cavity made of two highly reflective spherical mirrors separated by the distance L and having respectively a reflection coefficient R at the wavelength of laser. The Figure 1-5 shows the principle of the CRDS technique.

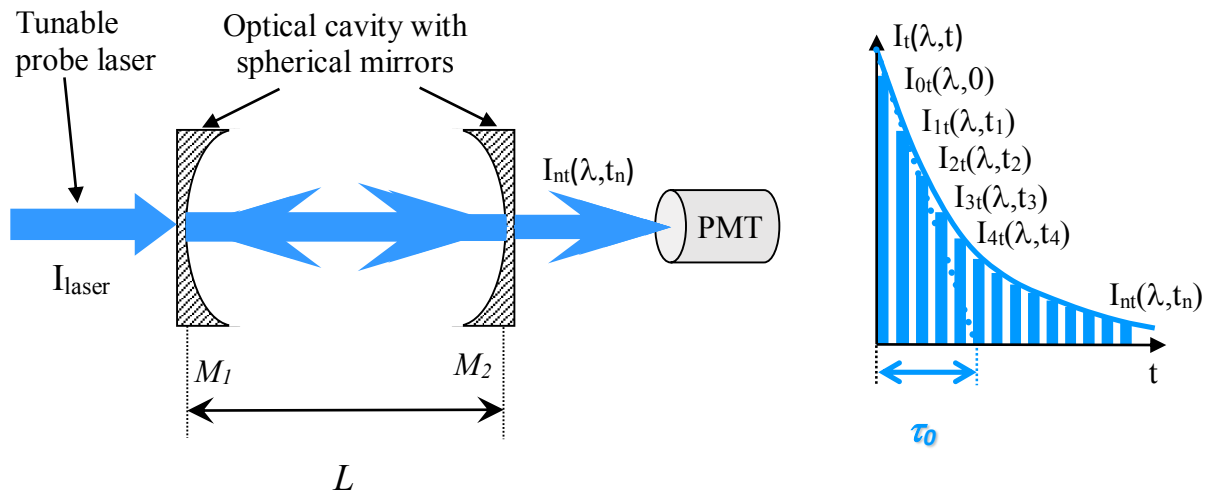


Figure 1-5: Scheme of the description of the so-called “Photon bullet model” of the pulse CRD technique.

Each time the pulse laser reaches the mirror’s surface, there is a reflection and a transmission. If we suppose that there is no absorption and scattering losses in the cavity, the intensity $I_{0t}(\lambda, 0)$ of the first pulse passing through the cavity could be written as, T being the transmission coefficient:

$$I_{0t}(\lambda, 0) = I_{laser} T^2 \quad (1-5)$$

After one round trip, the intensity of the second pulse is given:

$$I_{1,t}(\lambda, t_1) = I_{laser} TRRT = I_{0,t}(\lambda, 0) R^2 \quad (1-6)$$

with $t_1 = 2L/c = \Delta t$ being the round trip time. One more round trip takes place, the third pulse’s intensity will be:

$$I_{2t}(\lambda, t_2) = I_{laser} T(RR)^2 T = I_{1,t}(\lambda, t_1) R^2 \quad (1-7)$$

whereby $t_2 = t_1 + \Delta t = 2 \Delta t$

So, after $n+1$ completed round trips, the intensity of pulse on the detector will become:

$$I_{n+1,t}(\lambda, t_{n+1}) = I_{laser} T(RR)^{n+1} T = I_{n,t}(\lambda, t_n) R^2 \quad (1-8)$$

in which $t_{n+1} = t_n + \Delta t$, then:

$$I_{n+1,t}(\lambda, t_n + \Delta t) = I_{n,t}(\lambda, t_n) R^2 \quad (1-9)$$

Since $\Delta t = \frac{2L}{c} \ll 1$ we have:

$$I_{n+1,t}(\lambda, t_{n+1}) = I_{n+1,t}(\lambda, t_n + \Delta t) \approx I_{n,t}(\lambda, t_n) + \frac{dI_{n,t}(\lambda, t_n)}{dt} \Delta t \quad (1-10)$$

$$I_{n+1,t}(\lambda, t_{n+1}) - I_{n,t}(\lambda, t_n) = \frac{dI_{n,t}(\lambda, t_n)}{dt} \Delta t = I_{n,t}(\lambda, t_n) (R^2 - 1) \quad (1-11)$$

$$\Rightarrow \frac{dI_{n,t}(\lambda, t_n)}{I_{n,t}(\lambda, t_n)} = \frac{(R^2 - 1)}{\Delta t} dt \quad (1-12)$$

$$\Rightarrow \ln \frac{I_t(\lambda, t)}{I_{0,t}(\lambda, 0)} = \frac{(R^2 - 1)}{\Delta t} t \quad (1-13)$$

$$I_t(\lambda, t) = I_{0,t}(\lambda, 0) \exp \left(\frac{R^2 - 1}{\Delta t} t \right) = I_{0,t}(\lambda, 0) \exp \left(- \left(\frac{1 - R^2}{\Delta t} \right) t \right) \quad (1-14)$$

According to the calculation,

$$I_t(\lambda, t) = I_{0,t}(\lambda, 0) \exp\left(-\frac{t}{\tau_0(\lambda)}\right) \quad (1-15)$$

with

$$\tau_0(\lambda) = \frac{\Delta t}{1-R^2} = \frac{2L}{c(1-R^2)} \quad (1-16)$$

Here τ_0 is called the **ring-down time** and corresponds to the surviving mean time of the photons in the empty cavity. It is also called **mean lifetime of photons in the cavity**.

On the detector, generally a photomultiplier tube (PMT), in the case the round trip time $\Delta t = 2L/c$ of the pulse in the cavity is longer than laser pulse time – width δt , we observe a series of peaks separated with the same round trip time Δt and with exponential decay decreasing intensities. In the case that the round trip time $\Delta t = 2L/c$ of the laser pulse in the cavity is smaller than laser pulse time-width δt , we observe a continuous exponential decay (see chapter 4 for more details).

Because, in this technique, the reflection coefficient R is generally very close to 1, the transmission $T = 1 - R$ is very close to 0:

$$\tau_0(\lambda) = \frac{2L}{c(1-(1-T)^2)} \approx \frac{2L}{c(1-(1-2T))} = \frac{L}{cT} \quad (1-17)$$

$$\tau_0(\lambda) = \frac{L}{c(1-R)} \quad (1-18)$$

As an example, to give order of magnitude: if the length of the cavity $L = 100$ cm and the reflection coefficient $R = 99.99\%$ (typical value generally easily reached in the red), we obtained a ring down time value of $\tau_0 = 33.3 \mu\text{s}$ corresponding to an impressive effective mean distance done by the photons of $L_{\text{eff}} = c \tau_0 = 10$ km.

If we suppose now that absorbing species with an absorption coefficient $\alpha(\lambda)$ at the λ wavelength fill the cavity, following to the Figure 1-6.

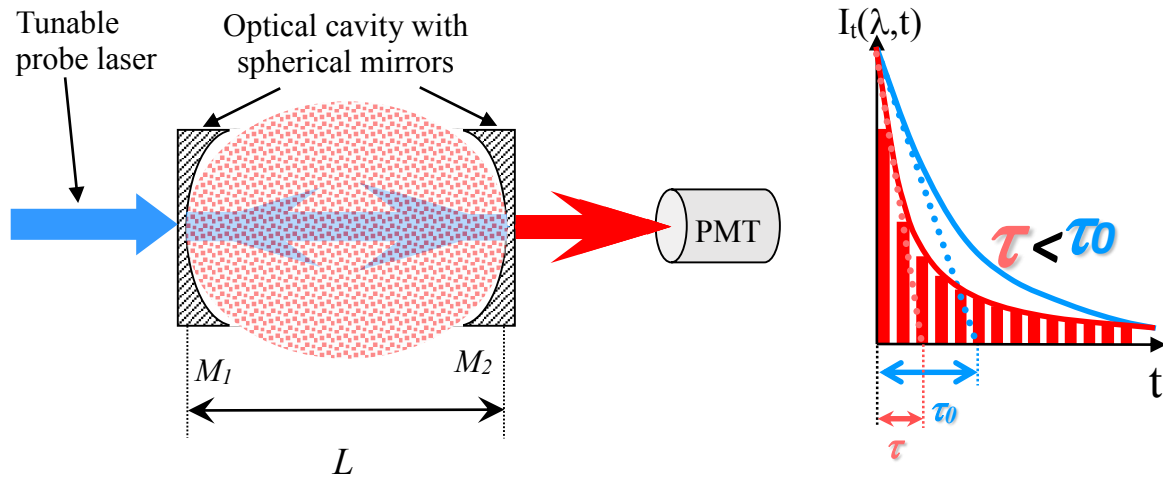


Figure 1-6: Cavity ring-down spectroscopy with absorbing species filling the cavity.

According to Beer-Lambert law, we can express now the intensity $I_{0,t}(\lambda, 0)$ of the first pulse passing through the cavity as:

$$I_{0,t}(\lambda, 0) = I_{laser} T e^{-\alpha(\lambda)L} T \quad (1-19)$$

After one round trip time, at the time t_1 :

$$I_{1,t}(\lambda, t_1) = I_{laser} T e^{-\alpha(\lambda)L} R e^{-\alpha(\lambda)L} R e^{-\alpha(\lambda)L} T \quad (1-20)$$

$$I_{1,t}(\lambda, t_1) = I_{0,t}(\lambda, t_0) R^2 e^{-2\alpha(\lambda)L} \quad (1-21)$$

So, after $n+1$ completed round trip, the intensity of pulse on the detector will become:

$$I_{n+1,t}(\lambda, t_{n+1}) = I_{n+1,t}(\lambda, t_n + \Delta t) = I_{n,t}(\lambda, t_{n,t}) R^2 e^{-2\alpha(\lambda)L} \quad (1-22)$$

$$\frac{dI_{nt}(\lambda, t_n)}{dt} \Delta t = I_{nt}(\lambda, t_n) (R^2 e^{-2\alpha(\lambda)L} - 1) \quad (1-23)$$

$$I_t(\lambda, t) = I_{0t}(\lambda, 0) e^{-\left(\frac{1-R^2 e^{-2\alpha(\lambda)L}}{\Delta t}\right)t} \quad (1-24)$$

$$I_t(\lambda, t) = I_{0t}(\lambda, 0) e^{-\frac{t}{\tau(\lambda)}} \quad (1-25)$$

And also

$$\tau(\lambda) = \frac{\Delta t}{1 - R^2 e^{-2\alpha(\lambda)L}} = \frac{\Delta t}{1 - (R e^{-\alpha(\lambda)L})^2} \quad (1-26)$$

If the reflection coefficient R of mirror is very close to 1 and if the losses represented by $2\alpha(\lambda)d$ are much smaller than 1 (i.e. weak absorption), also:

$$\tau(\lambda) = \frac{\Delta t}{1 - (1-T)^2 (1 - 2\alpha(\lambda)d)} \approx \frac{\Delta t}{1 - (1-2T)(1 - 2\alpha(\lambda)d)} = \frac{2L}{c(2T + 2\alpha(\lambda)d)} \quad (1-27)$$

Ring-down time is also given:

$$\tau(\lambda) = \frac{L}{c(T + \alpha(\lambda)d)} \quad (1-28)$$

When there is some absorbing species in the cavity, the intensity decreases also with an exponential decay, but the ring-down time is smaller, due to the absorption coefficient. The photons absorbed by the species are lost for the laser pulse and because of these additional losses the ring-down time is smaller.

From equation (1-18) and (1-28) we can extract the value of:

$$\frac{1}{\tau(\lambda)} - \frac{1}{\tau_0(\lambda)} = \frac{c(1-R + \alpha(\lambda)d)}{L} - \frac{c(1-R)}{L} = \frac{c\alpha(\lambda)d}{L} \quad (1-29)$$

If the cell is entirely filled by the absorbing species ($L=d$), the absorption coefficient of the species at λ wavelength is also easily deduced by the formula:

$$\alpha(\lambda) = \frac{1}{c} \left(\frac{1}{\tau(\lambda)} - \frac{1}{\tau_0(\lambda)} \right) \quad (1-30)$$

Because we are able to extract from this technique the 2 ring-down time values $\tau(\lambda)$ and $\tau_0(\lambda)$ respectively with and without absorbing species, we are also able to give the absolute absorption coefficient of the species at the wavelength λ .

1.2.3.2. Advantages and disadvantages of the CRDS technique

❖ Advantages of the CRDS technique

Like the classical absorption technique, CRDS is a noninvasive quantitative absorption technique.

$$\alpha(\lambda) = N\sigma(\lambda) = \frac{1}{c} \left(\frac{1}{\tau(\lambda)} - \frac{1}{\tau_0(\lambda)} \right) \quad (1-31)$$

If the absorption cross-section of the species is known for the wavelength λ , we can also extract the number density N of the species from the absorption coefficient measured with this experiment. On the contrary, if the density N of the species is known, we can extract from $\alpha(\lambda)$, the absorption cross-section of the species.

The minimum detectable absorption in CRDS can be provided as below:

$$\alpha_{\min}(\lambda) = \Delta\alpha(\lambda) = \frac{1}{c} \left(\frac{\Delta\tau_0}{(\tau_0(\lambda))^2} + \frac{\Delta\tau}{(\tau(\lambda))^2} \right) \approx \frac{1}{c\tau_0(\lambda)} \left(\frac{2\Delta\tau}{\tau(\lambda)} \right) = \frac{1-R}{L} \left(\frac{2\Delta\tau}{\tau(\lambda)} \right) = \frac{2T}{L} \left(\frac{\Delta\tau}{\tau(\lambda)} \right) \quad (1-32)$$

The smallest absorption coefficient which can be determined is proportional to the mirror transmission and inversely proportional to the length of cavity. It is directly positively proportional to a constant fractional change in time $\frac{\Delta\tau}{\tau(\lambda)}$. Therefore, it can also be asserted that the absorption coefficient is independent of the intensity fluctuation of the source.

With a simple CRDS set-up, a minimum absorption coefficient of $4 \cdot 10^{-6} \text{ cm}^{-1}$ can be easily achieved with for example $R=99.9 \%$, $L=50 \text{ cm}$ and $\frac{\Delta\tau}{\tau(\lambda)} = 10 \%$.

❖ Disadvantage of the CRDS technique

The highly reflective mirrors possess a narrow bandwidth. Indeed, the reflection coefficient R of the mirrors depends on the wavelength: $R(\lambda)$. Normally, the mirrors' bandwidth is about 50 nm in the visible region (see Figure 1-7). However, when the reflection coefficient R of the mirrors becomes bigger in value, the bandwidth will be narrower, leading to the fact that we will only be able to measure in a smaller range.

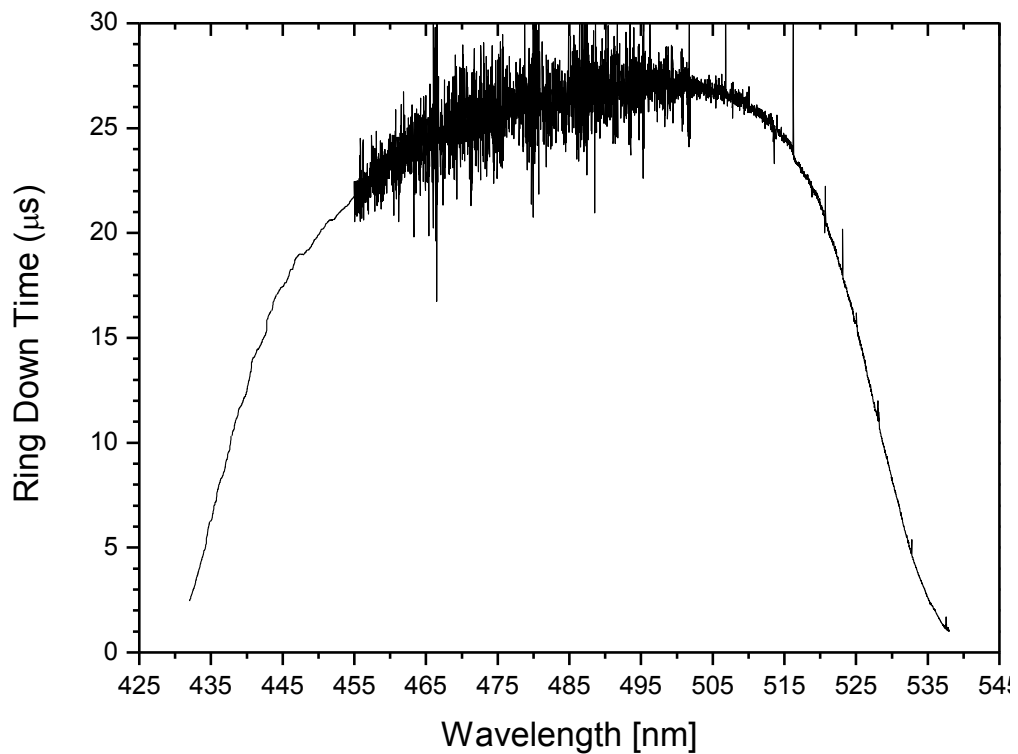


Figure 1-7: Ring down time's curve obtained for the OPO laser coupled with Ring-Down Cavity. This OPO laser (MOPO-730 from Spectra-Physics) has a bandwidth of about $\sim 0.25 \text{ cm}^{-1}$. The huge range of scan is from 430 nm to 540 nm.

Another disadvantage is that in case the range of the absorption features is unknown, exploration may not be performed by CRDS due to the limited scan range.

The mirror contamination will (dramatically) reduce the sensitivity of this technique due to the necessary high reflection coefficient R of the mirrors, which puts constraints on the sample cell.

The higher the reflection coefficient R of the mirrors is, the more expensive the price of the mirrors will be.

❖ **Some typical values:**

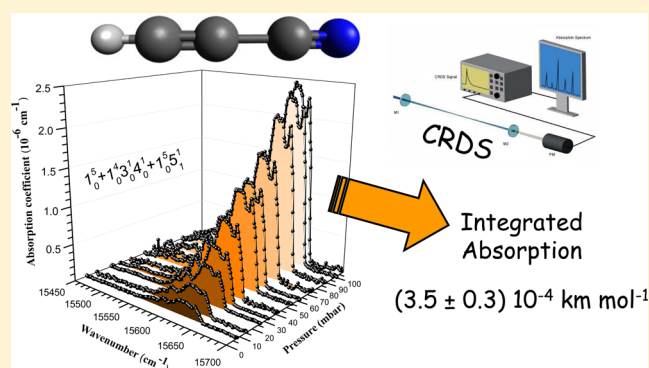
If $L = 1$ m, $R=99.99$ % and $\frac{\Delta\tau}{\tau(\lambda)} = 1\%$ (the lowest achievable variation detection in conventional CRDS) , according to formula 1-32, it is easy to obtain $\alpha_{\min} \sim 2 \cdot 10^{-8} \text{ cm}^{-1}$, comparing to the result achieved by the direct absorption technique, at best 10^{-4} cm^{-1} for $L=1$ m. Besides, if $N = 2.4 \cdot 10^{16} \text{ cm}^{-3}$ ($P = 1$ mbar) is given, and $\alpha_{\min} \sim 10^{-8} \text{ cm}^{-1}$, then according to formula 1-31, we can calculate the absorption cross-section of the sample $\sigma_{\min} \sim 5 \cdot 10^{-25} \text{ cm}^2$.

With typical molecular electric-dipole allowed rovibronic transitions the absorption cross-section is $\sigma \sim 10^{-18} \text{ cm}^2$, according to formula 1-31 the detectable number density (molecules per unit volume) of the absorber is $N_{\min} \sim 10^{10} \text{ cm}^{-3}$ and corresponds to ~ 0.5 ppbv.

Typical molecular electric-dipole forbidden but magnetic-dipole allowed rovibronic transition as for example the O_2 molecule on its $b \sum_g^+ \leftarrow X^3 \sum_g^-$ transition or typical molecular high vibrational absorption overtones transition if $\sigma \sim 10^{-25} \text{ cm}^2$, we can then obtain $N_{\min} = 10^{17} \text{ cm}^{-3}$ (corresponding to $P_{\min} \sim 5$ mbar).

Cavity Ring Down Spectroscopy Measurements for High-Overtone Vibrational Bands of HC₃NStéphane Douin,^{*,†} Marcin Gronowski,[‡] Nicolas Lamarre,[†] Viet-Tiep Phung,[†] Séverine Boyé-Péronne,[†] Claudine Crépin,[†] and Robert Kołos[‡][†]Institut des Sciences Moléculaires d'Orsay, UMR8214, CNRS, Université Paris-Sud, Bât. 210, F-91405 Orsay Cedex, France[‡]Institute of Physical Chemistry of the Polish Academy of Sciences, Kasprzaka 44, 01-224 Warsaw, Poland

ABSTRACT: Overtone ($5\nu_1$ and $6\nu_1$) and combination ($4\nu_1 + \nu_3$ and $4\nu_1 + \nu_2$) vibrational bands of gaseous HC₃N, located in the visible range (14 600–15 800 and 17 400–18 600 cm⁻¹), were investigated by cavity ring-down absorption spectroscopy. The $5\nu_1 + \nu_3$ and $5\nu_1 + \nu_2$ combinations as well as the $6\nu_1 + \nu_5 - \nu_5$ hot overtone band have also been identified, on the basis of previous overtone assignments. Absolute integrated intensity values and the ensuing oscillator strengths have been measured here for the first time; f values are typically confined between 4×10^{-12} and 7×10^{-11} . For the even weaker $5\nu_1 + \nu_2$ combination band, the oscillator strength was estimated as 9×10^{-13} . The values concerning CH-stretch overtones ($n\nu_1$) are similar to those found in the literature for HCN and C₂H₂, the molecules with sp-hybridized carbon atoms. Data presented here may prove useful for studying the photochemistry triggered with visible or near-IR radiation within the atmospheres of certain Solar System bodies, including Titan.



INTRODUCTION

HC₃N (cyanoacetylene, cyanoethyne, propynenitrile) is a molecule of astrophysical interest. It has been detected in the interstellar medium^{1–4} and cometary atmospheres,⁵ in the atmosphere of the biggest Saturn's moon Titan,⁶ and also in extragalactic sources.⁷ As the first member of the cyanopolyyne family, HC₃N plays an important role in the complex network of chemical reactions taking place in these diverse environments penetrated with UV and cosmic rays; cyanopolyynes are related to a whole range of unsaturated free radicals, and also to large chemical structures, like the polymeric ones present in the Titan's atmosphere (*tholins*), responsible for its characteristic orange haze.

Overtone frequencies strongly depend on the attractive part of the potential energy surface (PESs), whereas overtone intensities depend on its repulsive part.⁸ Experimental studies of highly excited vibrational states can therefore provide information on the shape (anharmonicity) of a PES at a considerable distance from its minimum, as well as on phenomena like internal vibrational redistribution or unimolecular reactions. Emission from highly excited vibrational states has been observed for hot ($T \geq 1500$ K) astronomical objects, including some gaseous disks surrounding young stars.⁹ Moreover, overtones are of importance for the Terrestrial atmospheric photochemistry,¹⁰ and supposedly also for the atmospheres of other Solar System bodies, including Titan. Cross sections for electronic absorptions (i.e., typically, those involving UV quanta) are usually orders of magnitude higher

than for vibrational overtone transitions; these latter, however, may provide the gate toward the photochemistry triggered with visible or near-IR radiation (of note, the maximum of solar emission lies in the visible).

The cavity-ring down spectroscopy (CRDS) technique has already been used to measure, for some molecules, the absolute absorption cross sections of high vibrational overtones, in particular those of CH stretching modes, located in the visible range. To our knowledge, Romanini et al.¹¹ were the first to record, with CRDS, the $n\nu_{\text{CH}}$ ($n = 5, 6$, and 7) overtone transitions and related combination bands in the case of the HCN molecule (17 500–23 000 cm⁻¹ range). Romanini et al.¹² also measured the ($5\nu_{\text{CH}} + \nu_{\text{C}\equiv\text{C}}$) combination band of acetylene, near 17 500 cm⁻¹. Kleine et al.¹³ have investigated the $6\nu_{\text{CH}}$ overtone of benzene, at 16 550 cm⁻¹, and measured the corresponding oscillator strength. DeMille et al.¹⁴ obtained the oscillator strength for the $6\nu_{\text{CH}}$ overtone bands of propane, *n*-butane, and neopentane. The phase-shift CRDS technique has been employed by Lewis et al.^{15,16} to measure the absolute absorption strength corresponding to the $5\nu_{\text{CH}}$ and/or $6\nu_{\text{CH}}$ overtone bands of ethylene, ethane, propane, *n*-butane, *n*-pentane, isobutene, and neopentane. For all above listed $5\nu_{\text{CH}}$ and $6\nu_{\text{CH}}$ bands, oscillator strengths on the order of 10^{-11} to 10^{-10} have been found.

Received: June 19, 2015

Revised: July 24, 2015

Many spectroscopic investigations devoted to gaseous HC₃N have been carried out during the last decades, but quantitative data concerning absolute integrated intensities of vibrational overtone transitions, located beyond IR range, are missing.

In the following section (Previous Studies) we sum up the characteristics of vibrational absorption bands already reported for HC₃N. The instrumentation and theory employed in this paper are described in the Experimental and Theoretical Methods. Respective spectra, data analysis procedures, and ensuing quantitative results are presented in the Results and Discussion.

■ PREVIOUS STUDIES

Infrared Spectroscopy. The first infrared study of HC₃N was carried out by Turrell et al.¹⁷ in 1957; they have measured the low-resolution absorption spectrum in the 450–3400 cm⁻¹ frequency region. The first high-resolution IR data were obtained by Mallinson and Fayt,¹⁸ who recorded the origins of bands corresponding to all seven fundamental vibrational modes (four stretches and three doubly degenerate bending modes). They have also measured the ro-vibrational absorption spectra of overtone, combination, and hot bands in the 1800–6500 cm⁻¹ range. Mallinson and Fayt's results concerning the central wavenumbers of fundamental vibrational bands are reported in Table 1.

Table 1. Fundamental Vibrational Modes of Gaseous HC₃N, after Mallinson and Fayt¹⁸

mode	vibration	symmetry	IR band center (cm ⁻¹)
ν_1	C—H str.	σ	3327.372
ν_2	C \equiv N str. ^a	σ	2273.996
ν_3	C \equiv C str. ^a	σ	2079.306
ν_4	C—C str.	σ	863.5
ν_5	HCC bend.	π	663.209
ν_6	CCN bend.	π	498.5
ν_7	CCC bend.	π	222.402

^aHighly delocalized modes.

Yamada et al. have appended the high-resolution results of Mallinson and Fayt¹⁸ with new data concerning the fundamental and hot bands of the ν_3 ^{19,20} and ν_2 ²¹ modes, as well as the ν_5 and ν_6 fundamentals.²² Arié et al.²³ analyzed 22 ro-vibrational bands including ν_5 , ν_6 , and the associated hot bands. Later on, Yamada et al.²⁴ recorded the $2\nu_5$ (or 5_0^2 ; this notation, preferentially used throughout the paper, indicates the mode number together with respective initial and final vibrational quantum numbers) overtone band and several hot bands in the 450–730 cm⁻¹ range, whereas Winther et al.²⁵ reinvestigated the ν_1 band system around 3327 cm⁻¹, carefully analyzing 12 hot bands. All above listed IR spectroscopic studies have been accomplished with the classical absorption technique, at room temperature.

Near-Infrared and Visible Spectroscopy. At higher frequency values (above 9500 cm⁻¹, i.e., in the near-IR and visible ranges), the first absorption study has been reported in 1984 by Hall.²⁶ In this impressive and complete work, Hall recorded, at room temperature, the visible absorption bands due to 1_0^n overtones ($n = 3–6$) and several associated combination bands for a range of HCCR derivatives (R = H, CN, CH₃, CD₃, CF₃, and (CH₃)₃). To ease the discussion for this series of molecules, he chose to use a nonstandard numbering of the stretching modes (different from that

adopted in Table 1), namely ν_1 for C—H, ν_2 for C \equiv C, ν_3 for C—C, and ν_4 for C \equiv N. Spectra were measured with the photoacoustic technique; the achieved resolution of 0.01 cm⁻¹ was imposed by the bandwidth of the applied dye laser. Of note, photoacoustic measurements do not allow for the absolute, direct determination of transition strengths. Gambogi et al.²⁷ have investigated the 1_0^3 band of HC₃N in a molecular beam, with a much higher resolution (5×10^{-4} cm⁻¹), employing a sequential, infrared/infrared double resonance excitation technique. By adding their value found for the origin of the 1_1^3 band to the 1_0^1 band center ($\nu_1 = 3327.372$ cm⁻¹, as reported by Mallinson and Fayt¹⁸), they have indirectly obtained 9666.703 cm⁻¹ as the center of the 1_0^3 band, a value very close to the one (9666.3 cm⁻¹) obtained by Hall²⁶ in photoacoustic measurements. More recently, the same 1_0^3 overtone of HC₃N has been reinvestigated and analyzed at room temperature by Cané et al.²⁸ with Fourier-transform and intracavity laser absorption spectroscopy (ICLAS) techniques. The band center of the second overtone of C—H stretching motion has been found at 9666.687 cm⁻¹.

Table 2 presents the wavenumbers corresponding to the centers of all identified fundamental, combination, overtone, and hot bands of HC₃N, in a broad range, extending from IR to green light. The listed values, extracted from the above-mentioned publications, were acquired with resolutions between 5×10^{-4} and 4×10^{-2} cm⁻¹.

The lowest vibrational levels (ν_7 , ν_6 , ν_5) are non-negligibly populated in the usual experimental conditions; a simple Boltzmann law-based estimation indicates that only about one-third of HC₃N molecules are, at 300 K, in the ground vibrational state. Consequently, the observed fundamental, overtone and combination vibrational transitions may be accompanied by hot bands. This is well illustrated by a complicated system of spectral features around 3327 cm⁻¹, in the vicinity of the fundamental ν_1 band (1_0^1) investigated by Winther et al.²⁵ Corresponding entries are highlighted in Table 2; the observed hot bands were found to originate in $n\nu_7$, ν_6 , and ν_5 and in the combinations of ν_6 and ν_7 , i.e.: 1_0^{17n} ($n = 1–4$), $1_0^6 1_1$, $1_0^5 1_1$, $1_0^6 1_1^7$, $1_0^6 1_1^7 2$. The separation of these bands from 1_0^1 was smaller than 3.5 cm⁻¹, with the exception of $1_0^5 1_1$, where it amounted to ~ 20 cm⁻¹, indicating a strong coupling between ν_1 (CH stretch) and ν_5 (CCH bend) modes.

Integrated Bands and Oscillator Strengths. Several studies have been devoted to measuring, for HC₃N, the absolute integrated intensities of IR absorption bands in the region of fundamental vibrational transitions—indispensable for quantitative astrophysical considerations. The first measurements have been carried out in 1974 by Uyemura et al.²⁹ with a 10 cm pathway and a resolution of 1 cm⁻¹, at room temperature. They reported on integrated intensity of the 4 fundamental stretching modes and verified the linearity of these quantities versus pressure. Later on, Uyemura et al.³⁰ obtained the integrated intensity for the 3 fundamental bendings, at $T = 273$ K. Khelifi et al.³¹ have measured (with a Fourier-transform instrument, at 308 K) the integrated intensity of the main bands of HC₃N in the 300–3500 cm⁻¹ range, with a resolution of 4 cm⁻¹. The work was then completed³² by studying the variation of ν_1 , ν_2 , ν_5 , and ν_6 bands strength with temperature (225–325 K range). More recently, Jolly et al.³³ reported on a comprehensive study at a resolution of 0.5 cm⁻¹, where the integrated intensities of 12 overtone, hot, and combination bands have been measured in addition to 6 fundamental modes.

Table 2. Assignments and Wavenumbers for Fundamental, Combination, Overtone, and Hot Band Centers of Gaseous HC₃N within the 220–18 500 cm⁻¹ Range

band	band center (cm ⁻¹)	band	band center (cm ⁻¹)
7 ₀ ¹	222.402 ^a	2 ₀ 6 ₀ ¹	2764.827 ^a
6 ₀ ¹	498.5, ^a 498.8022, ^b 498.8015 ^c	1 ₀ 7 ₁ ⁰	3104.961 ^a
6 ₀ 7 ₁ ¹	[497.898–498.158] ^b	2 ₀ 4 ₀ 7 ₁ ¹	3133.362 ^a
	[497.86–498.6458–498.7854–498.7852] ^c		
6 ₁ ²	[499.411–514.399] ^b	2 ₀ 4 ₀ ¹	3132.973 ^a
	[499.38063–499.38046–514.37083] ^c		
5 ₁ ²	[649.78166–669.8163] ^c	1 ₀ 5 ₁ ¹	3307.354,^a 3307.3516^h
5 ₀ ²	663.209, ^a 663.22203, ^b 663.21458 ^c	1 ₀ 7 ₄ ¹	[3324.1921–3324.1802] ^h
5 ₀ 7 ₁ ¹	[662.80930–663.724–663.724–664.151] ^c	1 ₀ 6 ₁ 7 ₂ ²	3324.8790^h
5 ₀ 6 ₁ ¹	[663.154–663.160–663.726] ^c	1 ₀ 7 ₃ ³	[3324.9612–3324.9453] ^h
5 ₀ 7 ₂ ²	[663.618–663.620–664.246] ^c	1 ₀ 6 ₁ 7 ₁ ¹	[3325.6761–3325.6773] ^h
6 ₀ 7 ₀ ¹	720.73770 ^c	1 ₀ 7 ₂ ²	3325.763,^a [3325.7750–3325.7616]^h
4 ₀ ¹	863.5 ^a	1 ₀ 6 ₁ ¹	3326.4702^h
5 ₁ ³	1301.44908 ^d	1 ₀ 7 ₁ ¹	3326.560,^a 3326.5674^h
4 ₀ 7 ₁ ³	1309.29 ^d	1 ₀ ¹	3327.372,^a 3327.37085^h
4 ₀ 7 ₀ ²	1310.0627 ^d	1 ₀ 7 ₂ ³	[3548.035–3547.584–3547.133] ^a
5 ₀ ²	1312.991921 ^d	1 ₀ 7 ₁ ²	[3548.512–3548.035] ^a
5 ₀ 6 ₁ ¹	1313.53147 ^d	1 ₀ 7 ₀ ¹	3548.950 ^a
5 ₀ 7 ₁ ¹	1314.23951 ^d	1 ₀ 6 ₀ ¹	3825.271 ^a
3 ₀ 7 ₂ ²	2074.579 ^a	1 ₀ 5 ₀ ¹	3970.563 ^a
	[2074.57319–2074.57334–2074.58991] ^e		
3 ₀ 6 ₁ ¹	2076.203 ^a	3 ₀ ²	4146.692 ^a
3 ₀ 7 ₁ ¹	2076.941 ^a [2076.94077–2076.94039] ^e	2 ₀ ²	4529.233 ^a
3 ₀ ¹	2079.306, ^a 2079.30606, ^c 2079.305 ^f	1 ₀ 7 ₁ ¹	6550.870 ^a
1 ₀ 5 ₀ 7 ₁ ¹	[2262.842–2262.424] ^a	1 ₀ ²	6551.980 ^a
1 ₀ 5 ₀ ¹	2264.129 ^a	1 ₀ ³	9666.3, ⁱ 9666.703, ^j 9666.687 ^k
2 ₀ 6 ₁ ¹	2267.371, ^a 2267.37605 ^g	1 ₀ 3 ₀ ¹	11 737 ⁱ
2 ₀ 7 ₃ ³	[2267.48669–2267.51565–2267.51605] ^g	1 ₀ 2 ₀ ¹	11 950 ⁱ
2 ₀ 5 ₁ ¹	2268.112 ^a	1 ₀ ⁴	12 695.7 ⁱ
2 ₀ 7 ₂ ²	2269.649 ^a , 2269.65867 ^g	1 ₀ 4 ₀ ¹	13 545.2 ⁱ
2 ₀ 7 ₁ ¹	2271.810, ^a 2271.81254 ^g	1 ₀ 3 ₀ ¹	14 738 ⁱ
2 ₀ ¹	2273.996, ^a 2273.99539 ^g	1 ₀ 2 ₀ ¹	14 960 ⁱ
2 ₀ 7 ₂ ²	[2492.411–2490.595] ^a	1 ₀ ⁵	15 640 ⁱ
2 ₀ 7 ₀ ¹	2494.220 ^a	1 ₀ ⁶	18 450 ⁱ
3 ₀ 6 ₀ ¹	2574.703 ^a		

^aIn ref 18. ^bIn ref 22. ^cIn ref 23. ^dIn ref 24. ^eIn ref 20. ^fIn ref 19. ^gIn ref 21. ^hIn ref 25; these values, concerning the ν_1 band system around 3327 cm⁻¹ (bold font), are thoroughly discussed in the text. ⁱIn ref 26; band center positions derived from the intersections of *P* and *R* rotational envelopes. ^jIn ref 27. ^kIn ref 28.

Table 3 presents all reported integrated intensities values for the fundamental, combination, overtone, and hot absorption bands of HC₃N. The ensuing oscillator strengths, derived with eqs A4 and A5 (Appendix), are also provided. It should be recalled that the observed fundamental, overtone, and combination vibrational transitions are accompanied by hot bands, and that the used resolution (0.5–4 cm⁻¹) is not sufficient to distinguish the inner substructure of these latter.

Theoretical Investigations. The best quantum chemical predictions regarding the fundamental vibrational frequencies of cyanoacetylene have been given by Botschwina.³⁴ Systematic theoretical studies on IR intensities of fundamental vibrational transitions in the homologous series of cyanopolynes (including HC₃N) have also been performed.³⁵ Overtone and combination modes of HC₃N required the application of a more advanced theoretical approach;^{36,37} frequencies and intensities have been given for the first, second, and third ν_1 overtone (the intensity of the latter was predicted as 3.1×10^{-3} km mol⁻¹). Holme and Hutchinson,³⁸ who investigated, with SCF calculations, the anharmonic interaction of 1₀⁵ and 1₀3₀4₀¹

modes, concluded that it could not be treated as a classical Fermi resonance case, given the weakness of coupling between the two modes. The proposed interaction mechanism³⁹ involved the potential extracted from available spectroscopic data; other vibrational states, mainly 1₀2₀¹, 1₀4₀¹, 1₀5₀¹, and 1₀4₀¹, were indicated as the ones mediating the interaction between 1₀⁵ and 1₀3₀4₀¹, leading to line broadening and to the loss of rotational structure.

EXPERIMENTAL AND THEORETICAL METHODS

Principles of the CRDS Technique. Review papers^{40–43} describe the cavity ring-down phenomenon, introduced to spectroscopy by O’Keefe and Deacon in 1988.⁴⁴ The technique generally consists in measuring the decay rate of a laser pulse (having the wavelength ν in cm⁻¹) sent into a rigid optical cavity made of two highly reflective spherical mirrors. Successive reflections from mirror surfaces cause an exponential decay of light collected at the exit:

Table 3. Frequencies, Absolute IR Intensities, and Oscillator Strengths for Several Fundamental, Combination, Overtone, and Hot Bands of HC₃N, As Reported in the Literature (Original Values Listed in Bold)

band	band center (cm ⁻¹)	absolute integrated intensity			temp (K)
		cm ⁻² atm ⁻¹	km mol ⁻¹	oscillator strength	
7 ₀ ¹	223.5	0.8 ± 0.2	0.18 ± 0.04^a	(3.4 ± 0.8) × 10 ⁻⁸	273
6 ₀ ¹	499.2	36 ± 5	8.0 ± 1.2^a	(1.5 ± 0.2) × 10 ⁻⁶	273
	500	30.9 ± 1.7^b	7.8 ± 0.4	(1.47 ± 0.08) × 10 ⁻⁶	308
	500	52.15–37.04^c	9.0–12.7	(1.7–2.4) × 10 ⁻⁶	225–325
	498.8	39.0 ± 1.9^d	9.5 ± 0.5	(1.8 ± 0.1) × 10 ⁻⁶	296
5 ₀ ¹	663.7	305 ± 46	68.4 ± 10.3^a	(1.3 ± 0.2) × 10 ⁻⁵	273
	663	199 ± 9^b	50 ± 2	(9.4 ± 0.4) × 10 ⁻⁶	308
	663	225.79–249.51^c	54.8–60.6	(1.0–1.1) × 10 ⁻⁵	225–325
	663.2	268.6 ± 7^d	65 ± 2	(1.22 ± 0.03) × 10 ⁻⁵	296
6 ₀ ¹ 7 ₀ ¹	711–727	12.1 ± 0.7^b	3.1 ± 0.2	(5.7 ± 0.3) × 10 ⁻⁷	308
	720.3	12.1 ± 0.9^d	2.9 ± 0.2	(5.5 ± 0.4) × 10 ⁻⁷	296
4 ₀ ¹	862	0.68 ± 0.03^d	(1.65 ± 0.07) × 10 ⁻¹	(3.1 ± 0.1) × 10 ⁻⁸	296
	863	~0.25	~0.06^e	~10 ⁻⁸	293
5 ₀ ¹ 7 ₀ ¹	878	0.8 ± 0.1^b	0.20 ± 0.02	(3.8 ± 0.5) × 10 ⁻⁸	308
6 ₀ ²	1013	2.2 ± 0.7^b	0.56 ± 0.02	(1.0 ± 0.3) × 10 ⁻⁷	308
	1013	1.72 ± 0.21^d	0.42 ± 0.02	(7.8 ± 0.5) × 10 ⁻⁸	296
4 ₀ ¹ 7 ₀ ¹	1090	0.32 ± 0.05^d	(7.8 ± 0.1) × 10 ⁻²	(1.5 ± 0.2) × 10 ⁻⁸	296
5 ₀ ¹ 6 ₀ ¹	1163	0.11 ± 0.02^d	(2.7 ± 0.5) × 10 ⁻²	(5.1 ± 0.9) × 10 ⁻⁹	296
5 ₀ ² 5 ₀ ¹ 7 ₀ ³	1322–1305	69.5 ± 1.8^b	17.6 ± 0.5	(3.30 ± 0.09) × 10 ⁻⁶	308
	1314	70.5 ± 3.5^d	17.1 ± 0.4	(3.21 ± 0.06) × 10 ⁻⁶	296
5 ₀ ³	1970	0.09 ± 0.02^d	(2.2 ± 0.5) × 10 ⁻²	(4.1 ± 0.9) × 10 ⁻⁹	296
3 ₀ ¹	2068–2085	8.5 ± 0.3^b	2.15 ± 0.08	(4.0 ± 0.2) × 10 ⁻⁷	308
	2079	8.0 ± 1.0^d	1.9 ± 0.2	(3.6 ± 0.5) × 10 ⁻⁷	296
	2077	8.0 ± 1.0	1.93 ± 0.29^e	(3.6 ± 0.5) × 10 ⁻⁷	293
	2263–2279	38.3 ± 1.1^b	9.7 ± 0.3	(1.82 ± 0.05) × 10 ⁻⁶	308
2 ₀ ¹	2274	40.7 ± 2.2^d	9.9 ± 0.5	(1.9 ± 0.1) × 10 ⁻⁶	296
	2263–2279	39.84–31.10^c	9.68–7.55	(1.42–1.82) × 10 ⁻⁶	225–325
	2272	41 ± 6	9.92 ± 1.49^e	(1.9 ± 0.3) × 10 ⁻⁶	293
	2494	1.38 ± 0.07^d	(3.4 ± 0.2) × 10 ⁻¹	(6.3 ± 0.3) × 10 ⁻⁸	296
3 ₀ ¹ 6 ₀ ¹	2575	0.71 ± 0.04^d	(1.7 ± 0.1) × 10 ⁻¹	(3.2 ± 0.2) × 10 ⁻⁸	296
2 ₀ ¹ 5 ₀ ⁰	2665	0.52 ± 0.04^d	(1.3 ± 0.1) × 10 ⁻¹	(2.4 ± 0.2) × 10 ⁻⁸	296
2 ₀ ¹ 6 ₀ ¹	2766	1.25 ± 0.15^d	(3.0 ± 0.4) × 10 ⁻¹	(5.7 ± 0.7) × 10 ⁻⁸	296
1 ₀ ¹ 7 ₀ ⁰	3104	2.6 ± 0.25^d	(6.3 ± 0.7) × 10 ⁻¹	(1.2 ± 0.1) × 10 ⁻⁷	296
2 ₀ ¹ 4 ₀ ¹	3133	2.6 ± 0.25^d	(6.3 ± 0.7) × 10 ⁻¹	(1.2 ± 0.1) × 10 ⁻⁷	296
1 ₀ ¹	3318–3336	274 ± 15^b	69 ± 4	(1.30 ± 0.07) × 10 ⁻⁵	308
	3327	249.4 ± 12^d	61 ± 3	(1.14 ± 0.05) × 10 ⁻⁵	296
	3318–3336	253.12–215.10^c	52.2–61.5	(0.98–1.15) × 10 ⁻⁵	225–325
	3327	251 ± 38	60.4 ± 9.1^e	(1.1 ± 0.2) × 10 ⁻⁵	293
1 ₀ ¹ 7 ₀ ¹	3549	1.47 ± 0.07^d	(3.6 ± 0.2) × 10 ⁻¹	(6.7 ± 0.3) × 10 ⁻⁸	296

^aIn ref 30. ^bIn ref 31. ^cIn ref 32; maximal and minimal integrated intensity values are given, for the temperature range 225–325 K. ^dIn ref 33. ^eIn ref 29.

$$I(t, \nu) = I(0, \nu) \exp\left(\frac{-t}{\tau(\nu)}\right) \quad (1)$$

where $I(0, \nu)$ is the laser intensity at $t = 0$ (i.e., intensity of light entering the cavity) and $\tau(\nu)$ is the lifetime of photons within the cavity, also called the ring-down time constant. When the cavity is empty (i.e., there is no absorption and no light-scattering), the corresponding ring-down time constant $\tau_0(\nu)$ depends only on the speed of light c , and on two parameters: the mirror reflectivity $R(\nu)$ and the cavity length L :

$$\tau_0(\nu) = \frac{L}{c(1 - R(\nu))} \quad (2)$$

When an absorbing species is filling the entire cavity, the ring-down time decreases due to the extinction of light:

$$\tau(\nu) = \frac{L}{c(1 - R(\nu) + \alpha(\nu)L)} \quad (3)$$

where $\alpha(\nu)$ is the extinction coefficient of the species at a given wavelength ν (equivalent to the absorption coefficient, if scattering of light can be neglected; $\alpha(\nu)$ can then be substituted by the product of the absorption cross section $\sigma(\nu)$ and the number density of absorber molecules N). Finally:

$$\frac{1}{\tau(\nu)} - \frac{1}{\tau_0(\nu)} = \alpha(\nu)c = \sigma(\nu)Nc \quad (4)$$

By measuring the ring-down time constant $\tau_0(\nu)$ for an empty cavity, the time constant $\tau(\nu)$, and the pressure of absorbers in a filled cavity (proportional to the number density in a given level), it is therefore possible to obtain the absolute absorption cross section $\sigma(\nu)$. Importantly, the technique is not

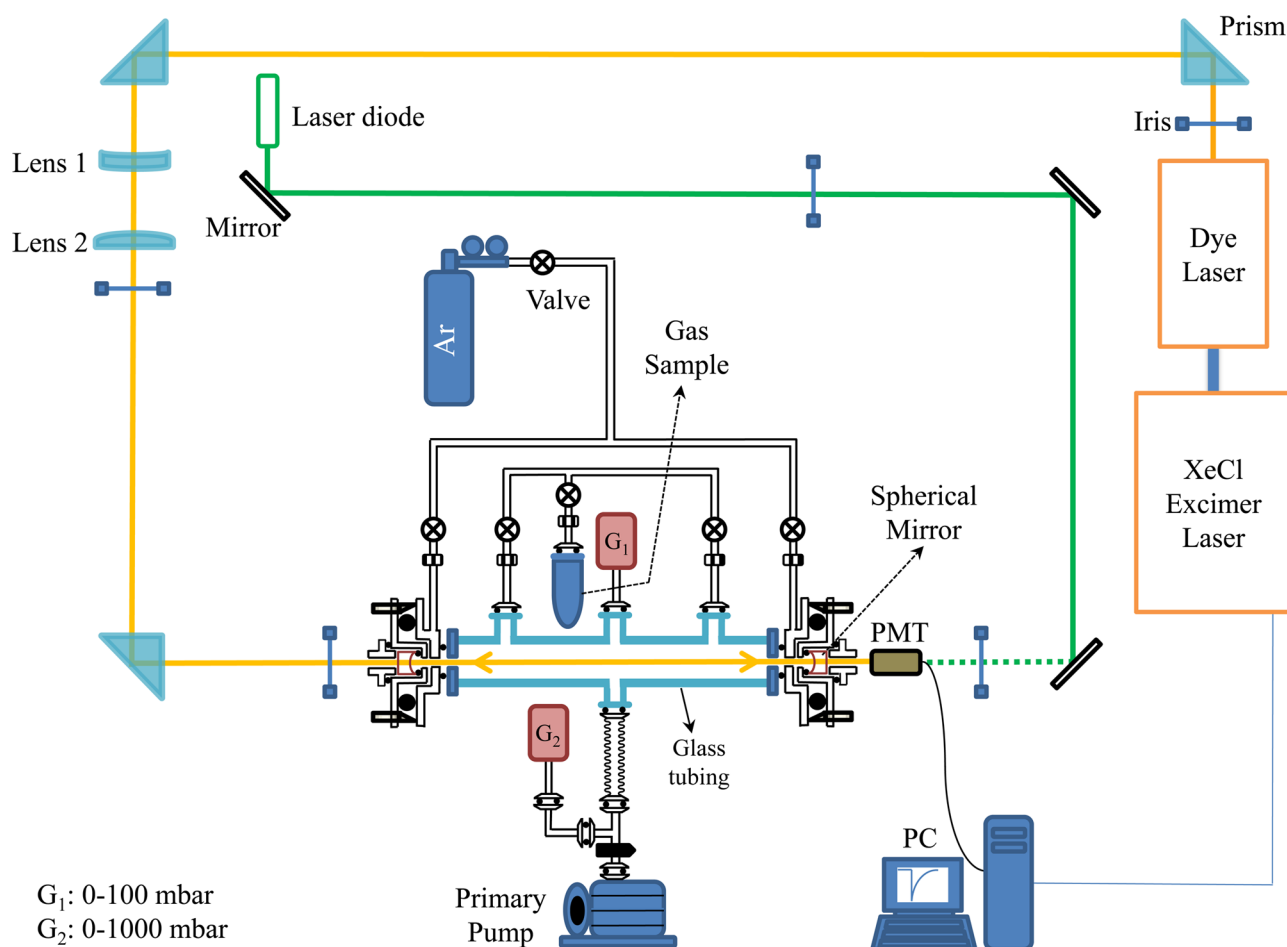


Figure 1. Experimental setup for room-temperature absolute intensity measurements of weak absorption bands.

sensitive to any shot-to-shot laser intensity fluctuations, as these do not alter the measurement of light decay corresponding to a single laser pulse. These features make it a technique of choice for quantitative studies of extremely weak vibrational overtone and combination absorption bands.

Probe Beam. Our experimental setup is shown in Figure 1. We used a pulsed XeCl (308 nm) excimer laser (Coherent, *CompexPro*; typical pulse energy of 300 mJ, pulse width of 15 ns, repetition rate 10 Hz) to pump a dye laser (Lambda Physik, LPD 3002), the latter operating with the following dyes (Exciton): DCM in methanol or ethanol for the range around 660 nm, Rhodamine 610 in methanol around 630 nm, and Coumarine 540A in ethanol for the 550 nm region. The dye laser pulse energy at the CRDS cavity entrance, after about 20 m propagation from the laser output, was about 0.5 mJ. In this configuration, no spatial filtering of the probe beam was necessary because all transverse electromagnetic modes, except TEM_{00} , were eliminated due to their divergence. Wavelength of the dye laser pulse was controlled with a wavelength meter (Ångstrom WS/6 High Precision), and the calibration accuracy was checked by the observation of known atmospheric absorptions. The measured laser bandwidth was $0.12 \pm 0.02 \text{ cm}^{-1}$.

Ring-Down Cavity. Two pairs of CRDS mirrors (Layertec GmbH, curvature radius $R_C = 1 \text{ m}$) were used, covering the two regions of interest: 525–575 nm and 620–680 nm, with reflection coefficients R not lower than 99.98% and 99.99%, respectively. The distance between mirrors was fixed at $L =$

67.5 cm to meet the stability condition for the cavity ($g = 1 - (L/R_C) = 0.325 \in [0-1]$).⁴⁵ Homemade mirror holders allowed for the fine adjustments, without breaking the vacuum. The highest ring-down time constant τ_0 reached for the empty cavity was about 17.5 μs for the first set of mirrors (at ca. 560 nm) and about 35 μs for the second one (around 665 nm). The light leaving the cavity was collected behind the rear mirror by a photomultiplier tube (Hamamatsu H10721-01). The signal was processed, without any prior amplification, by a computer equipped with a high-speed acquisition card (Zteck 4441 PCI, 14 bits, 800MS/s).

Data Acquisition and Treatment. A homemade *LabVIEW*-based (National Instruments, *LabVIEW* 8.5) data acquisition system was used to extract real-time ring-down time constants corresponding to every single laser pulse. This was accomplished by approximating the experimental signals with single-exponential decays $y(t, \nu) = A \exp(-t/\tau(\nu))$, in time-windows located between $0.2\tau_0$ and $7.5\tau_0$ (corresponding, respectively, to about 80 and 0.05% of the transmitted light intensity). Any possible residual offset, due to constant signals, was subtracted, after averaging the intensity of 100 points typically located at $15\tau_0$. The dye laser wavelength was scanned during the experiment, but each point of the resultant $\tau(\nu)$ spectrum corresponded to an averaging over several tens of laser pulses. Such a preliminary treatment of data was fast enough to be performed during the experiment. Once the acquisition was completed, the nonlinear Levenberg–Marquardt procedure could be employed to accomplish the post-

treatment of averaged decay data by fitting them with the $y(t, \nu) = A \exp(-t/\tau(\nu)) + B$ function, which takes into account, via the B parameter, possible constant offsets. The use of a monoexponential function for fitting the average of monoexponential decays is justified, provided that the dispersion of ring-down decay times is small. The latter condition is fulfilled because, typically, the pulse-to-pulse deviation of the decay times did not exceed 3% (i.e., $\Delta\tau/\tau(\nu) \leq 0.03$). The ensuing high S/N ratio allowed for reaching very low absorption coefficient values, namely $\alpha_{\min}(\nu) = [(1 - R(\nu))/L][\Delta\tau/\tau(\nu)]_{\min} \approx 5 \times 10^{-8} \text{ cm}^{-1}$. When averaged over 100 laser pulses, the $\alpha_{\min}(\nu)$ further decreased to approximately $5 \times 10^{-9} \text{ cm}^{-1}$; this corresponds to the minimal detectable absorption cross section of approximately $2 \times 10^{-27} \text{ cm}^2$ for a pressure of 100 mbar (or a number density of $2.4 \times 10^{18} \text{ cm}^{-3}$).

The Sample. HC_3N was synthesized with a slightly modified method of Miller and Lemmon.⁴⁶ Gaseous compound was introduced to the CRDS cavity, via a needle valve, from a room-temperature container (295 K), where it was present at the pressure of approximately 480 mbar.⁴⁷ The 50 cm long cavity (ISO KF DN40 tube) was made of Pyrex glass to minimize the adsorption of molecules. Inside the cavity, HC_3N pressure was controlled in the range 1–150 mbar, with the aid of capacitance manometers (Pfeiffer Vacuum CMR363 10 mbar, CMR362 100 mbar, or MKS Baratron 100 Torr). Static mode (i.e., no inert gas purging the surface of mirrors) was chosen, to improve the stability of HC_3N pressure inside the cavity. No degradation of mirror surfaces occurred, as was evidenced by the day-to-day constancy of the τ_0 ring-down time.

Ab Initio Calculations. An all-electron correlation approach and the CFOUR⁴⁸ software was applied. Geometry optimizations were carried out for linear cyanoacetylene molecules, using the CCSD(T)^{49–51} variant of the coupled cluster method (featuring single, double, and triple excitations, the latter treated perturbatively), with a correlation-consistent triple- ζ basis set (cc-pVTZ).⁵² Anharmonic (VPT2)^{53–56} calculations were performed at the same level of theory. The energy of a vibrational level was described by

$$E(n_1, n_2, \dots, n_7) = hc \left(\sum_{i=1}^7 \omega_i \left(n_i + \frac{g_i}{2} \right) + \sum_{\substack{i,j=1 \\ i \leq j}}^7 x_{ij} \left(n_j + \frac{g_j}{2} \right) \left(n_i + \frac{g_i}{2} \right) \right) \quad (5)$$

with n_i representing the vibrational quantum numbers, h and c the Planck constant and the speed of light, ω_i the harmonic vibration frequency of the i th mode (g_i -fold degenerate), and x_{ij} the anharmonicity constants, these latter measuring the degree of coupling between modes i and j .

RESULTS AND DISCUSSION

Spectra. The two panels of Figure 2 show absorption spectra measured at room temperature in the red and green ranges (see the figure caption for additional details). Ring-down times were transformed to absorption coefficient values with the aid of eq 4, and to absolute absorption cross sections by dividing the absorption coefficient by the number density N ; it was possible to avoid more complicated procedures,^{57,58} because the observed absorption bands were very broad compared to the frequency bandwidth (0.12 cm^{-1}) of the

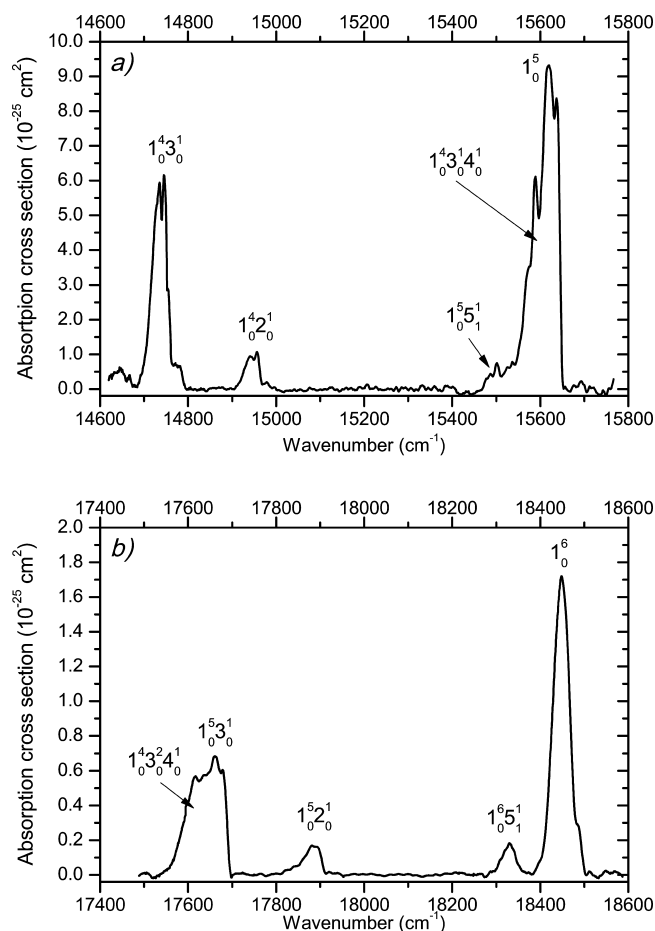


Figure 2. Absolute absorption cross section of HC_3N in the ranges of 14 600–15 800 cm^{-1} (panel a) and 17 400–18 600 cm^{-1} (panel b); spectra recorded at 295 K, with the HC_3N pressure of 150 and 80 mbar, respectively. Probe laser scanned with a step of 0.05 nm.

probe laser. Given this lack of fine spectral features, it was in principle sufficient to scan the laser wavelength with a step of 0.05 nm ($1.1\text{--}1.7 \text{ cm}^{-1}$). In fact, the absolute absorption cross section of Figure 2 should be interpreted as an effective value, corresponding to room temperature (295 K), assuming the number density of absorbers equal to N , even for the hot bands.

Spectra presented in Figure 2 exhibit seven differently shaped absorption bands, their half-width ranging from 35 to 100 cm^{-1} , approximately. Corresponding absorption cross sections vary between, approximately, 10^{-26} and 10^{-24} cm^2 . The most intense feature of Figure 2a, located around $15 600 \text{ cm}^{-1}$, was analyzed by Hall²⁶ in his photoacoustic study, at room temperature, without absolute intensity determinations. The complexity of shape, and the half-width of about 62 cm^{-1} , advocated for the presence of intruding combination bands; Hall²⁶ suggested a Fermi resonance between the 1^5_0 overtone and $1^4_{3_0}4^1_0$ combination-overtone band. This possible anharmonic interaction has also been theoretically investigated by Hutchinson³⁹ (see Previous Studies section). The most intense feature of Figure 2b, located around $18 450 \text{ cm}^{-1}$, was assigned by Hall to the 1^6_0 overtone band. The shape of this band is less complex than the one observed at $15 600 \text{ cm}^{-1}$ (suggesting the absence of an interacting combination band). Its half-width, however, is huge: about 43 cm^{-1} , i.e., much larger than the separation of P and R branches maxima, expected for a typical allowed, unresolved ro-vibrational band. Such a separation can be

estimated⁵⁹ here as $2.35 \cdot (B \text{ (cm}^{-1}) \cdot T \text{ (K)})^{1/2}$, i.e., 16 cm^{-1} at room temperature. Broadening of the $15\,600 \text{ cm}^{-1}$ band (and of the other overtone features observed here) is partly due to unavoidable hot bands, originating in significant room-temperature populations of the lowest fundamental and combination levels (see *Previous Studies* section). Short lifetimes of the relevant excited states may also contribute to the discussed broadening.

Noteworthy, energy of the highest overtone band investigated in this work (1_0^6 around $18\,500 \text{ cm}^{-1}$) is well below the lowest dissociation threshold of HC_3N corresponding to the H-loss channel: $\text{HC}_3\text{N} \rightarrow \text{C}_3\text{N} + \text{H}$. This threshold has been experimentally estimated as higher than ca. $41\,000 \text{ cm}^{-1}$ by Titarchuk et al.⁶⁰ The respective ab initio fission energy, derived by Luo et al.,⁶¹ was $45\,600 \text{ cm}^{-1}$.

The details of 1_0^5 and 1_0^6 overtone bands are shown in *Figure 3*. The 1_0^5 feature has been recorded with a wavelength step of 0.005 nm (adjusted accordingly to the dye laser bandwidth of 0.12 cm^{-1}). For the 1_0^6 feature, where the shape is simpler, the step of 0.01 nm (0.34 cm^{-1}) was much bigger than the laser bandwidth. *Figure 3* provides also the comparison of our CRDS spectra to those obtained by Hall²⁶ in a photoacoustic

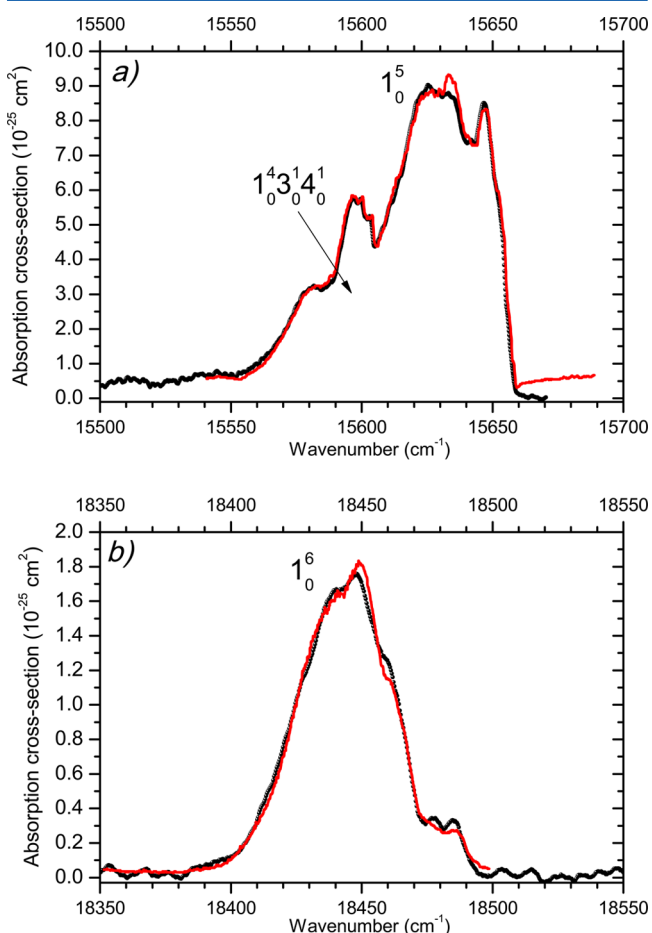


Figure 3. Detailed profiles of the 1_0^5 (panel a; HC_3N pressure of 98 mbar, probe laser wavelength step of 0.005 nm) and 1_0^6 (panel b; 83.5 mbar, step 0.01 nm) overtone bands (black traces, this work). Red-line traces, with arbitrary intensity scales (vertically adjusted to match present CRDS data) correspond to spectral features observed by Hall²⁶ in room-temperature photoacoustic experiments on diluted HC_3N samples [14% vol in 233 mbar of He (a) or 25% vol in 267 mbar of He (b)].

experiment (red line in the figure). Importantly, the bandwidth of a continuous-wave dye laser employed by Hall, 0.01 cm^{-1} , was by an order of magnitude narrower than in our measurements (see the figure caption for additional details). In spite of different instrumental resolutions, our spectra and the ones obtained by Hall²⁶ are remarkably similar, proving the intrinsic character of observed band profiles. Moreover, the measured profiles did not show, within the investigated pressure range, any signs of pressure broadening. The typical spectral bandwidth of our probe laser (0.12 cm^{-1}), confronted with the magnitude of rotational constant ($B_0 = 0.152 \text{ cm}^{-1}$)⁶² in the ground electronic ($^1\Sigma^+$) and vibrational state of HC_3N , and with the similarity of $B(5\nu_1)$ and $B(6\nu_1)$ values to that of B_0 (the respective vibration-rotation coupling constant α equals $0.2443 \times 10^{-3} \text{ cm}^{-1}$)³⁴ could suggest the possibility of resolving some individual ro-vibrational lines within 1_0^5 or 1_0^6 overtone bands. This did not prove to be the case; the loss of rotational structure in 1_0^n overtone bands, beyond $n = 4$, has already been reported by Hall,²⁶ and interpreted as the result of coupling between the vibrational levels corresponding to involved stretching modes and the dense bath of other states, at this very high degree of vibrational excitation, above $\sim 15\,000 \text{ cm}^{-1}$. Such couplings are responsible for the internal vibrational redistribution (IVR) mechanism, leading to the broadening of spectral bands via decrease of the lifetime of high ro-vibrational states and, possibly, to the disappearance of rotational structure.

The two weaker bands visible in *Figure 2a*, located to the red side of 1_0^5 , have been assigned to the combination bands: $1_0^4 3_0^1$ and $1_0^4 2_0^1$. These features were also observed by Hall²⁶ who did not, however, present the corresponding spectra.

New overtone/combination bands have been detected in the course of the present study (*Table 4*). These weak spectral features could be identified on the basis of previous overtone assignments. The one located around $17\,650 \text{ cm}^{-1}$ is very broad; its complex shape, with a steep high-frequency slope and the pattern of sub-bands, closely resembles the feature located around $15\,600 \text{ cm}^{-1}$ in which the anharmonic-interaction of levels 1_0^5 and $1_0^4 3_0^1 4_0^1$ has been discerned. Indeed, by introducing an additional ν_3 quantum, the two elements of the $17\,650 \text{ cm}^{-1}$ group may be tentatively interpreted as an anharmonic resonance pair $1_0^5 3_0^1 / 1_0^4 3_0^2 4_0^1$. A small band around $17\,900 \text{ cm}^{-1}$ can be assigned to $1_0^5 2_0^1$ (a contribution from $1_0^4 2_0^1 3_0^1 4_0^1$ cannot be ruled out).

The examination of spectra in *Figure 2* reveals yet another weak feature (at $18\,330 \text{ cm}^{-1}$), located about 120 cm^{-1} to the red of the expected 1_0^6 overtone. As remarked in the *Previous Studies* section, our room-temperature spectra are expected to contain some hot bands originating in thermally populated ν_5 , ν_6 , and ν_7 modes, as well as in the multiples or combinations of these three, with joint energy not exceeding several hundred wavenumbers. The gap Δ_{GH} between ground-state-originating 1_0^n overtones and associated hot bands (the latter stemming from $m_i \nu_i + m_j \nu_j$ levels, with $i, j = 5-7$, and m_i, m_j being either zero or a small integer value) increases with the anharmonicity constants x_{1i} and x_{1j} and with n :

$$\Delta_{\text{GH}} = x_{1i} n m_i + x_{1j} n m_j = n(x_{1i} m_i + x_{1j} m_j) \quad (6)$$

Given the half-width of overtone bands observed here (at least 35 cm^{-1}), one can derive approximately 7 cm^{-1} as the lowest x_{1i} and x_{1j} value that still permits for the separation of a hot band from pure 1_0^5 or 1_0^6 overtones. The most important of the relevant anharmonicity constants have been derived by Winther et al.²⁵ in the course of their high-resolution infrared

Table 4. Assignments, Wavenumbers, and Absolute Absorption Intensities for the Identified Overtone and Combination Bands of Gaseous HC₃N, As Presently Derived with the CRDS Technique^a

main contributing transitions	band maximum (cm ⁻¹)	band origin (cm ⁻¹ , ref 26)	absolute integrated intensity		
			cm ⁻² atm ⁻¹	km mol ⁻¹	oscillator strength <i>f</i>
1 ₀ ⁴ 3 ₀ ¹	14 745	14 738	(6.5 ± 0.5) × 10 ⁻⁴	(1.6 ± 0.1) × 10 ⁻⁴	(2.9 ± 0.2) × 10 ⁻¹¹
1 ₀ ⁴ 2 ₀ ¹	14 957	14 960	(8.8 ± 0.6) × 10 ⁻⁵	(2.1 ± 0.2) × 10 ⁻⁵	(4.0 ± 0.3) × 10 ⁻¹²
1 ₀ ⁵ 5 ₁ ^{1*} c	15 500				
1 ₀ ⁵ * ^c and 1 ₀ ⁴ 3 ₀ ¹ 4 ₀ ^{1*} * ^{b,c}	15 619	15 640	(1.46 ± 0.1) × 10 ⁻³	(3.5 ± 0.3) × 10 ⁻⁴	(6.6 ± 0.5) × 10 ⁻¹¹
1 ₀ ⁵ 3 ₁ ¹	17 661		(1.5 ± 0.2) × 10 ⁻⁴	(3.6 ± 0.5) × 10 ⁻⁵	(7.0 ± 1.0) × 10 ⁻¹²
1 ₀ ⁵ 2 ₀ ¹	17 882		~2 × 10 ⁻⁵	~5.0 × 10 ⁻⁶	~0.9 × 10 ⁻¹²
1 ₀ ⁶ 5 ₁ ^{1**d}	18 330				
1 ₀ ⁶ ** ^d	18 452	18 450	(2.1 ± 0.3) × 10 ⁻⁴	(4.9 ± 0.7) × 10 ⁻⁵	(9.2 ± 1.0) × 10 ⁻¹²

^aSeveral band origins measured with the photoacoustic technique are listed for comparison. ^bThe two listed bands are in an anharmonic resonance. ^cIntegration limits encompass all asterisked spectral features. ^dIntegration limits encompass both doubly asterisked spectral features.

Table 5. Experimental and Theoretically Derived (VPT2-CCSD(T)/cc-pVTZ) Anharmonicity Constants (cm⁻¹) Related to the CH Stretching Mode (ν₁) of Cyanoacetylene

	Winther et al. ^a	this work	
		experiment	theory VPT2-CCSD(T)/cc- pVTZ
x ₁₇	-0.8020 ± 0.0005		-1.2
x ₁₆	-0.9006 ± 0.0002		-1.4
x ₁₅	-20.0192 ± 0.0002	-20.0 ± 0.5 ^b	-14
x ₁₄			0.5
x ₁₃			-6.1
x ₁₂			-1.9
x ₁₁		-50 ± 2 ^c	-55

^aIn ref 25. Measurements were accurate enough to reflect a contribution from second anharmonicity constants *y*_{ijk}. ^bValue extracted from the analysis presented in Figure 4a (see text). ^cValue extracted from the analysis presented in Figure 4b (see text).

study on the ν₁ band system; corresponding accurate values describing the couplings of CH stretching motion (ν₁) with the lowest frequency modes ν₇, ν₆, ν₅, are complemented in Table 5 with the results of our present *ab initio* predictions for x_{1i} (i = 1–7). An outstandingly high value of x₁₅ is to be noted. For the described CRDS experiment, these clues allowed us to expect the presence of two separate bands around the frequency of any ν₁ overtone, each consisting of multiple, unresolved elements. The first of these would be due to a pure 1₀ⁿ transition, with some contribution from ν₆- or ν₇-involving hot bands. The second, much weaker band, appearing at a slightly lower frequency, would then be caused by hot overtone transitions stemming either from the singly excited ν₅ mode or, possibly, from a combination of that latter with ν₆ or ν₇. Specifically, for the spectral feature at 18 330 cm⁻¹ and for the shoulder around 15 500 cm⁻¹, the expected major contributions are, respectively, the 1₀⁶5₁¹ and 1₀⁵5₁¹ hot bands. This assignment is enhanced by Hall's²⁶ tentative identification of the 1₀⁴5₁¹ band located about 75 cm⁻¹ to the red of the 1₀⁴ overtone, and by our careful analysis of Hall's data that led to discerning analogous red-shifted satellites accompanying the first and second overtones of ν₁. Figure 4a illustrates how the 1₀⁵5₁¹ – 1₀ⁿ wavenumber difference evolves as a function of *n*. Experimental errors were estimated by considering the width of involved spectral features and our capability of finding the positions of true maxima. The obtained correlation is almost perfectly linear, its slope gives x₁₅ = -20.0 ± 0.5 cm⁻¹, in agreement with the value reported by

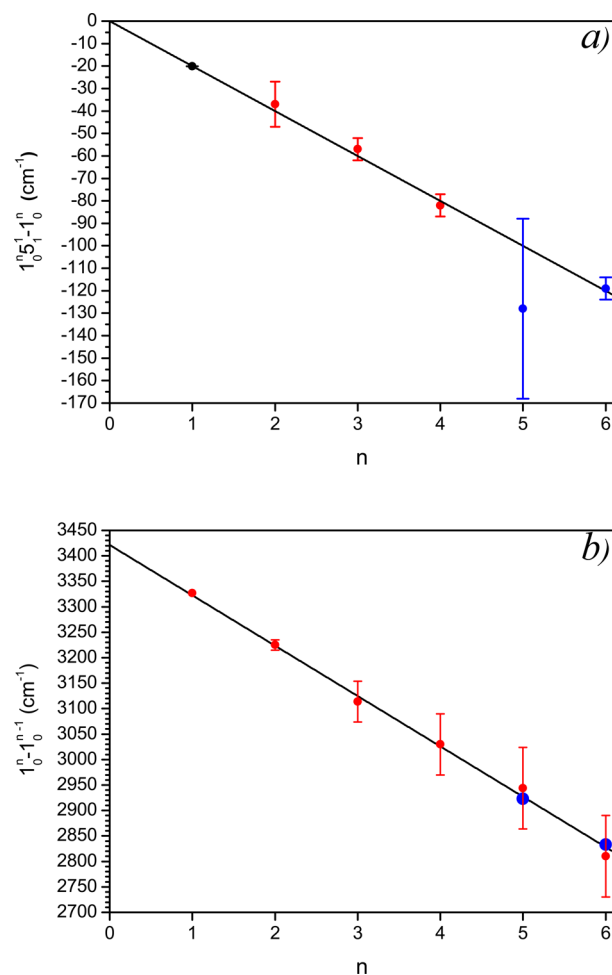


Figure 4. (a) Evolution of the gap between pure overtone bands 1₀ⁿ and their hot bands 1₀⁵5₁¹, as a function of *n*; data extracted from the reports by Mallinson et al.¹⁸ and Winther et al.²⁵ (black circles) and Hall²⁶ (red circles) and from the present measurement (blue circles). (b) Wavenumber difference 1₀ⁿ – 1₀ⁿ⁻¹ between the consecutive overtones plotted versus *n*; data extracted from the work of Hall²⁶ (with estimated band origin frequencies; red circles) and from the present measurements (basing on band maxima; blue circles). See text for the discussion of errors.

Winther et al.²⁵ A mismatch visible for *n* = 5 obviously comes from the interaction of 1₀⁵ and 1₀⁴3₀¹4₀¹ levels, which complicates the band profile and spoils its resolution from 1₀⁵5₁¹; the corresponding entry has therefore not been included in the

derivation of x_{15} . The key anharmonicity constant x_{11} was obtained from the $1_0^n - 1_0^{n-1}$ energy difference plotted vs n (Figure 4b). The slope of an ensuing linear relation equals $2x_{11}$, leading to $x_{11} = -50 \pm 2 \text{ cm}^{-1}$, in very good agreement with our theoretical prediction (Table 5). Problems with finding the true origins of relevant bands did not permit us to reliably estimate minor anharmonicity constants x_{12} and x_{13} . A very small value predicted for x_{14} suggests virtually no coupling between the C–H and C–C stretches.

Assuming the Boltzmann distribution of all involved thermally populated vibrational states, one should anticipate the $1_0^5/1_0^5 5_1^1$ intensity ratio of approximately 12. Acceptably close to that is the measured $1_0^5/1_0^5 5_1^1$ value of 9 ± 3 (a similar estimation is not possible for the corresponding $5\nu_1$ bands, poorly resolved and overlapped with a Fermi-resonance component). The combined $1_0^5 + 1_0^5 5_1^1$ absolute integrated intensity (or oscillator strength; Table 4), refers to an effective value, characterizing all overtone transitions of the $n\nu_1$ family, originating either in the ground vibrational level or in low-lying, thermally excited levels.

Absolute Intensities. To verify the consistency of the present experimental data, we have analyzed the intensity of several overtone and combination bands, as a function of HC_3N pressure, in the range 8–108 mbar. Within the limits of Beer–Lambert approximation, proportionality of the absorption coefficient defined as $\alpha = 1/L \ln(I_0/I)$ or of the integrated absorption $\int \alpha(\nu) d\nu = 1/L \int \ln(I_0/I) d\nu$ to pressure (or concentration) of absorbing molecules is to be expected. As depicted by Figure 5a, the profile of the complex, most intense overtone band observed here, consisting mostly of 1_0^5 , $1_0^4 3_0^1 4_0^1$, and $1_0^5 5_1^1$, was found to preserve its shape for HC_3N pressures differing by 1 order of magnitude, thus confirming the absence of measurable pressure broadening effects. Quantitative conclusions can be drawn from Figure 5b, where the corresponding integrated absorption values are plotted against pressure. The two groups of points (red and black circles) of Figure 5b correspond to the data sets obtained with two different manometers (Experimental and Theoretical Methods), during separate experiments. The two groups can be fitted with practically the same linear function (slope of $1.44 \times 10^{-6} \text{ cm}^{-2} \text{ mbar}^{-1}$, corresponding to $1.46 \times 10^{-3} \text{ cm}^{-2} \text{ atm}^{-1}$), proving the credibility of collected results. At the temperature of $295 \pm 2 \text{ K}$, corresponding to our experimental conditions, the above-given slope value yields (with conversion formulas, eqs A4 and A5; see the Appendix) the absolute intensity value of $3.53 \times 10^{-4} \text{ km mol}^{-1}$ and the oscillator strength of 6.62×10^{-11} . To estimate the involved data acquisition and band integration errors, the measurement was repeated, at a fixed gas pressure, in several independent experimental runs; the resultant integrated intensity values were constant within 5%. Taking into account this finding, together with the quality of a linear fit of Figure 5b, we estimate the error to 7%, i.e., the effective value for combined 1_0^5 , $1_0^4 3_0^1 4_0^1$, and $1_0^5 5_1^1$ is $f = (6.6 \pm 0.5) \times 10^{-11}$.

The dependence of integrated intensity on HC_3N pressure has also been analyzed for several other overtone and combination bands. Respective plots are collected in Figure 6. Data points can clearly be fitted with straight lines, even though the scatter is substantial for weaker bands. The resultant (extracted from the slopes) absolute integrated intensities and oscillator strengths are listed in Table 4. Relative uncertainties for the absolute integrated intensities and oscillator strength

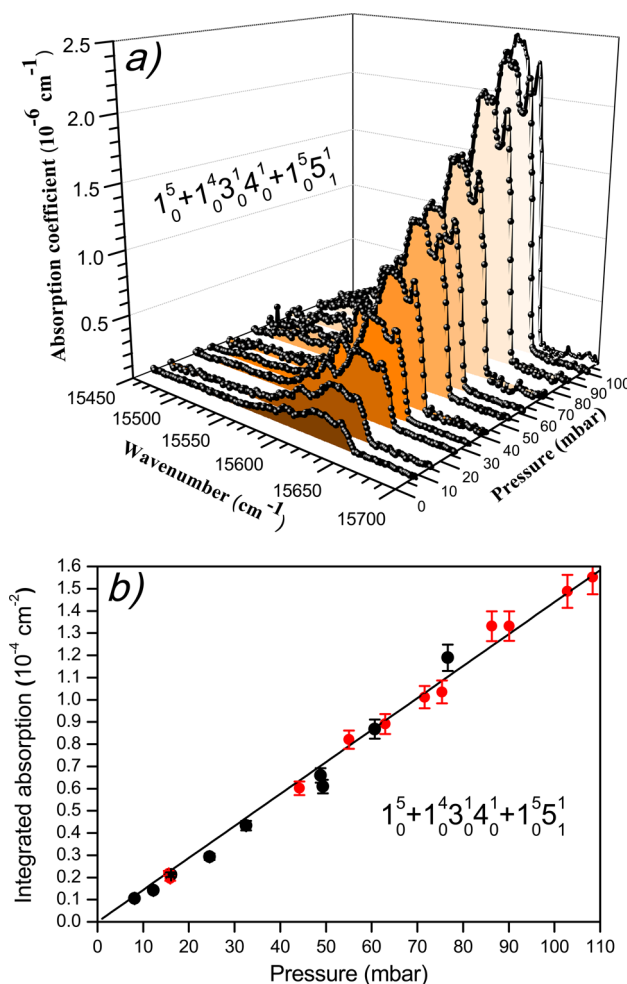


Figure 5. (a) Pressure dependence of absorption coefficient $\alpha(\nu)$ in the 1_0^5 vibrational overtone region of HC_3N . (b) Integrated absorption coefficient $\int \alpha(\nu) d\nu$ for the combined $1_0^5 + 1_0^4 3_0^1 4_0^1 + 1_0^5 5_1^1$ bands, plotted as a function of HC_3N pressure. Black and red circles mark data points coming from separate experimental runs, obtained with two different manometers. The estimated accuracy of integrated absorption coefficient determinations is 5%.

measurements appearing in Table 4, deduced from the linear fits, are about 7% for $1_0^4 3_0^1$ and $1_0^4 2_0^1$, and for the combined $1_0^5 + 1_0^4 3_0^1 4_0^1 + 1_0^5 5_1^1$ bands, whereas for $1_0^5 3_0^1$ and the combined $1_0^5 + 1_0^5 5_1^1$ bands the expected uncertainty is 13%. Intensity of $1_0^5 2_0^1$ was close to the detection limit of our system, not allowing for a reliable pressure dependence study; it was nevertheless possible to roughly estimate the strength of this feature on the basis of the spectrum presented in Figure 2.

Finally, it should be remarked that overtone oscillator strengths values derived here are similar to those found for other instances of CH stretches with sp-hybridized carbon atoms. Published data are scarce yet permit the comparison with HCN and C_2H_2 , presented in Table 6.

CONCLUSIONS

Visible vibrational absorption was investigated for gaseous HC_3N with the help of the cavity ring-down spectroscopy technique. Six overtone and combination bands, located in the visible range ($14\,600$ – $15\,800$ and $17\,400$ – $18\,600 \text{ cm}^{-1}$), have been recorded. New overtone/combination bands were observed here for the first time and identified on the basis of

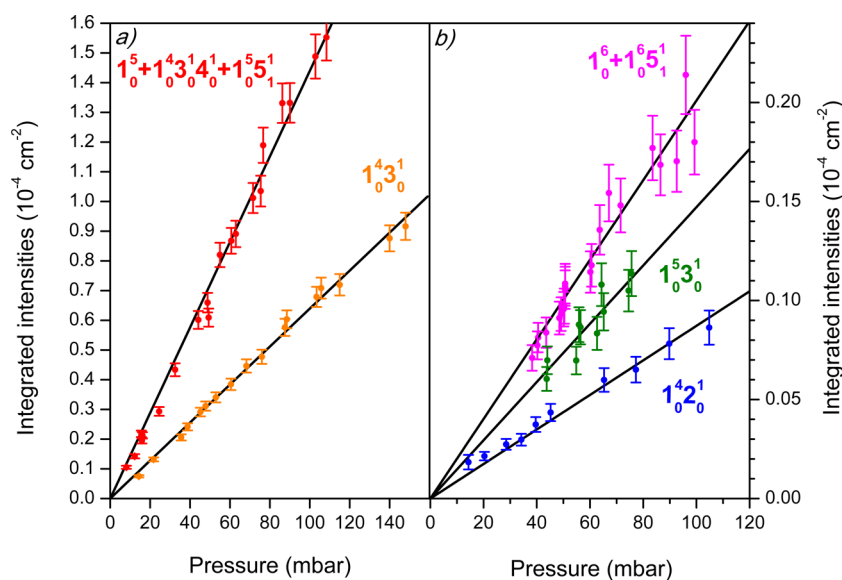


Figure 6. (a) Integrated absorption coefficient $\int \alpha(\nu) d\nu$ for the strongest overtone and combination bands: $1_0^5 + 1_0^4 3_0^1 4_0^1 + 1_0^5 5_1^1$ (red) and $1_0^4 3_0^1$ (orange), plotted against HC_3N pressure. The estimated relative error of integrated absorption coefficient determination is 7%. (b) Integrated absorption coefficient for three weaker overtone and combination bands: $1_0^6 + 1_0^5 5_1^1$ (magenta), $1_0^5 3_0^1$ (green), and $1_0^4 2_0^1$ (blue) plotted against HC_3N pressure. The estimated relative error is 13%. See Table 4 for the ensuing absolute intensity and oscillator strength values.

Table 6. Oscillator Strengths of Acetylene C—H Stretching Vibrational Transitions for the Fundamental (f_{01}) Mode, as Well as for the Fourth (f_{05}) and Fifth (f_{06}) Overtones

molecule		$f_{01}/10^{-5}$	$f_{05}/10^{-11}$	$f_{06}/10^{-11}$
hydrogen cyanide	$\text{H}-\text{C}\equiv\text{N}$	$1.01 \pm 0.02^{a,h}$	$3.28 \pm 0.8^{b,h}$	$0.490^{c,h}$
acetylene	$\text{H}-\text{C}\equiv\text{C}-\text{H}$	$1.32 \pm 0.01^{d,h}$	$7.1 \pm 0.2^{e,h}$	$0.90 \pm 0.8^{e,h}$
cianoacetylene	$\text{H}-\text{C}\equiv\text{C}-\text{C}\equiv\text{N}$	$1.14 \pm 0.05^{f,h}$	6.6 ± 0.5^g	0.92 ± 0.10^g

^aIn ref 63 and 64. ^bIn ref 65. ^cIn ref 11. ^dIn ref 66 value affected by a strong Fermi resonance, ^eIn ref 67. ^fIn ref 33. ^gThis work. ^hRecalculated from km mol^{-1} (eq A5).

previous overtone assignments. Anharmonic constants have been obtained by *ab initio* calculations and compared to the experimental values. Some of these are reported here for the first time, including the crucial x_{11} constant. A strong anharmonic interaction between the modes ν_1 and ν_5 is confirmed. A series of weak spectral features has been assigned to $1_0^n 5_1^1$ overtone hot bands ($n = 5, 6$ in the present spectra, and $n = 2, 3, 4$ in those reported by Hall²⁶).

Absolute integrated intensities of all observed bands have been measured, and the observed linear correlation of these values to HC_3N pressure has led to oscillator strengths for five overtone and combination bands. The latter strengths are similar to the ones found in literature for the respective overtones of other molecules featuring acetylene C—H overtone transitions.

To have a better insight into the potential energy surface characterizing the ground electronic state of HC_3N , it could be interesting to measure the oscillator strengths of spectral features in the 1_0^n regions ($n = 2, 3$ and 4), previously investigated by Hall²⁶ with the photoacoustic technique, and probably also of the ones that have still not been explored, i.e., $n > 6$. Experiments employing easily synthesized cyanoacetylene isotopologues DC_3N or HC_3^{15}N would permit more reliable spectral assignments, in particular for anharmonic resonance cases. Furthermore, coupling the CRDS instrumentation to the supersonic molecular jet technique would have the advantage of producing simpler, hot-band-free overtone spectra. The expected sensitivity, even though lower than in

typical CRDS experiments, should then allow for studying the 1_0^2 and 1_0^3 bands, this last one absorbing about 2 orders of magnitude stronger than 1_0^5 .

APPENDIX

Integrated Intensity and Oscillator Strength

It follows from the Beer–Lambert law, in the absence of saturation effects, that the absolute absorption intensity at a given wavenumber (cm^{-1}) can be expressed as the absorption cross section:

$$\sigma = \frac{1}{NL} \ln\left(\frac{I_0}{I}\right) \quad (\text{A1})$$

where N is the number of absorbing molecules per volume unit, L denotes the optical path, and I_0 and I are the incident and transmitted light intensities, respectively.

The integrated intensity A of a band extending from ν_i to ν_f is given by

$$A = \frac{1}{pL} \int_{\nu_i}^{\nu_f} \ln\left(\frac{I_0}{I}\right) d\nu \quad (\text{A2})$$

where p is the partial pressure of absorbing species. Alternatively

$$A' = \frac{1}{CL} \int_{\nu_i}^{\nu_f} \ln\left(\frac{I_0}{I}\right) d\nu \quad (\text{A3})$$

with C being the molar concentration of absorbers. Frequently used A and A' units are $\text{cm}^{-2} \text{atm}^{-1}$ and km mol^{-1} , respectively, with the conversion formula (for T expressed in Kelvin):

$$A' (\text{km mol}^{-1}) = \frac{T (K)}{1218.7} A (\text{cm}^{-2} \text{atm}^{-1}) \quad (\text{A4})$$

The related, dimensionless quantity is the oscillator strength f , readily obtained from the integrated intensity via

$$\begin{aligned} f &= 10^3 \frac{4\epsilon_0 m_e c^2}{N_A e^2} A' (\text{km mol}^{-1}) = 1.876 \times 10^{-7} A' (\text{km mol}^{-1}) \\ &= 1.54 \times 10^{-10} T (K) A (\text{cm}^{-2} \text{atm}^{-1}) \end{aligned} \quad (\text{A5})$$

where N_A is the Avogadro's number, e the electron's charge, ϵ_0 the permittivity of vacuum, m_e the electron's mass, c the speed of light, and T the temperature in Kelvin.

AUTHOR INFORMATION

Corresponding Author

*S. Douin. E-mail: stephane.douin@u-psud.fr.

Notes

The authors declare no competing financial interest.

ACKNOWLEDGMENTS

Authors acknowledge the financial support from the Campus Paris-Saclay Scientific Cooperation foundation *Digiteo Triangle de la Physique* (DOREMI, no. 2009-063T), the French-Polish Hubert Curien Programs *Polonium* (2011-2013), the International Project of Scientific Cooperation *PICS* (CNRS/PAN; No. 4717), and from the National Science Centre (Poland), project No. 2011/03/B/ST4/02763. Quantum chemical calculations were accomplished at the Interdisciplinary Centre for Mathematical and Computational Modelling, Warsaw University (grant No. G36-13).

REFERENCES

- Turner, B. E. Detection of Interstellar Cyanoacetylene. *Astrophys. J.* **1971**, *163*, L35–L39.
- Dickinson, D. F. Detection of Cyanoacetylene at 18 GHz. *Astrophys. Lett.* **1972**, *12*, 235–236.
- Mcgee, R. X.; Balister, M.; Newton, L. M. Interstellar Cyanoacetylene $J = 2-1$, $J = 4-3$ Transitions. *Mon. Not. R. Astron. Soc.* **1977**, *180*, 585–592.
- Gardner, F. F.; Winnewisser, G. Observations of $J = 1-0$ Transitions of C-13 Isotopic-Species of Cyanoacetylene (HCCCN) in Direction of Sagittarius B2. *Astrophys. J.* **1975**, *197*, L73–L76.
- Bockelee-Morvan, D.; Lis, D. C.; Wink, J. E.; Despois, D.; Crovisier, J.; Bachiller, R.; Benford, D. J.; Biver, N.; Colom, P.; Davies, J. K.; et al. New Molecules Found in Comet C/1995 O1 (Hale-Bopp) - Investigating the Link between Cometary and Interstellar Material. *Astron. Astrophys.* **2000**, *353*, 1101–1114.
- Kunde, V. G.; Aikin, A. C.; Hanel, R. A.; Jennings, D. E.; Maguire, W. C.; Samuelson, R. E. C_4H_2 , HC_3N and C_2N_2 in Titan's Atmosphere. *Nature* **1981**, *292*, 686–688.
- Mauersberger, R.; Henkel, C.; Sage, L. J. Dense Gas in Nearby Galaxies .3. HC_3N as an Extragalactic Density Probe. *Astron. Astrophys.* **1990**, *236*, 63–68.
- Medvedev, E. S. Towards Understanding the Nature of the Intensities of Overtone Vibrational Transitions. *J. Chem. Phys.* **2012**, *137*, 174307.
- Najita, J. R.; Doppmann, G. W.; Carr, J. S.; Graham, J. R.; Eisner, J. A. High-Resolution K-Band Spectroscopy of MWC 480 and V1331 Cyg. *Astrophys. J.* **2009**, *691*, 738–748.
- Donaldson, D. J.; Tuck, A. F.; Vaida, V. Atmospheric Photochemistry via Vibrational Overtone Absorption. *Chem. Rev.* **2003**, *103*, 4717–4729.
- Romanini, D.; Lehmann, K. K. Ring-Down Cavity Absorption Spectroscopy of the Very Weak HCN Overtone Bands with 6, 7, and 8 Stretching Quanta. *J. Chem. Phys.* **1993**, *99*, 6287–6301.
- Romanini, D.; Kachanov, A. A.; Sadeghi, N.; Stoeckel, F. CW Cavity Ring down Spectroscopy. *Chem. Phys. Lett.* **1997**, *264*, 316–322.
- Kleine, D.; Stry, S.; Lauterbach, J.; Kleinermanns, K.; Hering, P. Measurement of the Absolute Intensity of the Fifth CH Stretching Overtone of Benzene Using Cavity Ring-down Spectroscopy. *Chem. Phys. Lett.* **1999**, *312*, 185–190.
- DeMille, S.; Delaat, R. H.; Tanner, R. M.; Brooks, R. L.; Westwood, N. P. C. Comparison of CRDS to ICL-PAS and Phase-Shift CRDS Spectroscopies for the Absolute Intensities of C-H ($\Delta\nu_{\text{CH}} = 6$) Overtone Absorptions. *Chem. Phys. Lett.* **2002**, *366*, 383–389.
- Lewis, E. K.; Reynolds, D.; Li, X. C.; de Villele, G.; Leduc, C.; Cedeno, D. L.; Manzanares, C. Phase Shift Cavity Ring-down Measurement of C-H ($\Delta\nu = 6$) Vibrational Overtone Absorptions. *Chem. Phys. Lett.* **2001**, *334*, 357–364.
- Lewis, E. K.; Moehnke, C. J.; Manzanares, C. E. Phase Shift Cavity Ring down and FT-VIS Measurements of C-H ($\Delta\nu = 5$) Vibrational Overtone Absorptions. *Chem. Phys. Lett.* **2004**, *394*, 25–31.
- Turrell, G. C.; Jones, W. D.; Maki, A. Infrared Spectra and Force Constants of Cyanoacetylene. *J. Chem. Phys.* **1957**, *26*, 1544–1548.
- Mallinson, P. D.; Fayt, A. High Resolution Infra-Red Studies of HCCCN and DCCCN. *Mol. Phys.* **1976**, *32*, 473–485.
- Yamada, K.; Schieder, R.; Winnewisser, G.; Mantz, A. W. Diode-Laser Spectrum of HCCCN near $5 \mu\text{m}$. *Z. Naturforsch., A: Phys. Sci.* **1980**, *35*, 690–693.
- Yamada, K.; Winnewisser, G. Diode-Laser Spectrum of HCCCN near $5 \mu\text{m}$ - The Hot Band. *Z. Naturforsch., A: Phys. Sci.* **1981**, *36*, 23–29.
- Yamada, K.; Best, R.; Winnewisser, G. Diode-Laser Spectrum of -CN Stretching Band. *Z. Naturforsch., A: Phys. Sci.* **1983**, *38*, 1296–1308.
- Yamada, K. M. T.; Burger, H. The ν_5 and ν_6 Fundamental Bands of HCCCN. *Z. Naturforsch., A: Phys. Sci.* **1986**, *41*, 1021–1023.
- Arie, E.; Dang Nhu, M.; Arcas, P.; Graner, G.; Bürger, H.; Pawelke, G.; Khelifi, M.; Raulin, F. Analysis of Cyanoacetylene Spectra in the Mid-Infrared. *J. Mol. Spectrosc.* **1990**, *143*, 318–326.
- Yamada, K. M. T.; Moravec, A.; Niedenhoff, M.; Burger, H.; Winnewisser, G. The $2\nu_5$ Overtone Band of Cyanoacetylene by High Resolution FTIR Spectroscopy. *Z. Naturforsch., A: Phys. Sci.* **1996**, *51*, 27–35.
- Winther, F.; Klee, S.; Mellau, G.; Naim, S.; Mbosei, L.; Fayt, A. The ν_1 Band System of H-CC-CN (cyanoacetylene). *J. Mol. Spectrosc.* **1996**, *175*, 354–362.
- Hall, Randy Ray. Laser Photoacoustic Spectroscopy of Forbidden Transitions: Acetylene and Alkyne High Energy Vibrational States and Their Interactions (Intramolecular, Redistribution). *Rice University*, 1984.
- Gambogi, J.; Kerstel, E.; Yang, X. High-Resolution Spectrum of the $3\nu_1$ Band of Cyanoacetylene Obtained via Infrared/Infrared Double Resonance. *J. Mol. Spectrosc.* **1996**, *175*, 198–202.
- Cané, E.; Fusina, L.; Campargue, A.; Bürger, H. Intracavity Laser Absorption Spectroscopy and Fourier Transform Spectrum of the $3\nu_1$ Band Region of Cyanoacetylene. *J. Mol. Spectrosc.* **2009**, *253*, 25–29.
- Uyemura, M.; Maeda, S. Infrared Intensities of Stretching Fundamentals in Gaseous and Crystalline Cyanoacetylene. *Bull. Chem. Soc. Jpn.* **1974**, *47*, 2930–2935.
- Uyemura, M.; Deguchi, S.; Nakada, Y.; Onaka, T. Infrared Intensities of Bending Fundamentals in Gaseous HCCCN and DCCCN. *Bull. Chem. Soc. Jpn.* **1982**, *55*, 384–388.
- Khelifi, M.; Raulin, F.; Arie, E.; Graner, G. Absolute Intensity of the IR Bands of Propynenitrile. *J. Mol. Spectrosc.* **1990**, *143*, 209–211.

- (32) Khlifi, M.; Raulin, F.; Dangnhu, M. Integrated Band Intensity versus Temperature for the ν_1 , ν_2 , ν_5 , and ν_6 Bands of Cyanoacetylene. *J. Mol. Spectrosc.* **1992**, *155*, 77–83.
- (33) Jolly, A.; Benilan, Y.; Fayt, A. New Infrared Integrated Band Intensities for HC₃N and Extensive Line List for the ν_5 and ν_6 Bending Modes. *J. Mol. Spectrosc.* **2007**, *242*, 46–54.
- (34) Botschwina, P. Spectroscopic Properties of Interstellar Molecules: Theory and Experiment. *Phys. Chem. Chem. Phys.* **2003**, *5*, 3337–3348.
- (35) Vichiatti, R. M.; Haiduke, R. L. A. The Infrared Fundamental Intensities of Some Cyanopolynes. *Spectrochim. Acta, Part A* **2012**, *90*, 1–11.
- (36) Botschwina, P. Infrared Intensities of Polyatomic Molecules Calculated from SCEPTOR Dipole-Moment Functions and Anharmonic Vibrational Wavefunctions. I. Stretching Vibrations of the Linear Molecules HCN, HCP and C₂N₂. *Chem. Phys.* **1983**, *81*, 73–85.
- (37) Botschwina, P.; Schulz, B.; Horn, M.; Matuschewski, M. Ab Initio Calculations of Stretching Vibrational Transitions for the Linear Molecules HCN, HNC, HCCF and HC₃N up to High Overtones. *Chem. Phys.* **1995**, *190*, 345–362.
- (38) Holme, T. A.; Hutchinson, J. S. SCF Calculation of the Structure, Force Field, and Dipole Function of Cyanoacetylene. *Chem. Phys.* **1985**, *93*, 419–423.
- (39) Hutchinson, J. S. High-Energy Vibrational State of Cyanoacetylene - Variational and Perturbative Analysis of an Anharmonic Normal Mode. *J. Chem. Phys.* **1985**, *82*, 22–30.
- (40) Scherer, J. J.; Paul, J. B.; OKeefe, A.; Saykally, R. J. Cavity Ringdown Laser Absorption Spectroscopy: History, Development, and Application to Pulsed Molecular Beams. *Chem. Rev.* **1997**, *97*, 25–51.
- (41) Wheeler, M. D.; Newman, S. M.; Orr-Ewing, A. J.; Ashfold, M. N. R. Cavity Ring-down Spectroscopy. *J. Chem. Soc., Faraday Trans.* **1998**, *94*, 337–351.
- (42) Berden, G.; Peeters, R.; Meijer, G. Cavity Ring-down Spectroscopy: Experimental Schemes and Applications. *Int. Rev. Phys. Chem.* **2000**, *19*, 565–607.
- (43) Berden, G.; Engeln, R. In *Cavity Ring-Down Spectroscopy: Techniques and Applications*; Berden, G.; Engeln, R., Eds.; Wiley: New York, 2009.
- (44) O'Keefe, A.; Deacon, D. A. G. Cavity Ring-Down Optical Spectrometer for Absorption-Measurements Using Pulsed Laser Sources. *Rev. Sci. Instrum.* **1988**, *59*, 2544–2551.
- (45) Kogelnik, H.; Li, T. Laser Beams and Resonators. *Appl. Opt.* **1966**, *5*, 1550–1567.
- (46) Miller, F. A.; Lemmon, D. H. The Infrared and Raman Spectra of Dicyanodiacetylene, NCCCCCN. *Spectrochim. Acta Part A Mol. Spectrosc.* **1967**, *23*, 1415–1423.
- (47) Landolt-Bornstein. *Numerical Data and Functional Relationships in Science and Technology, Group IV*; Vol. 20, Vapor Pressure of Chemicals; Vol. C, Vapor Pressure and Antoine Constants for Nitrogen Containing Organics Compounds; Springer: Berlin, Heidelberg, New York, 2001.
- (48) Stanton, J. F.; Gauss, J.; Harding, M. E.; Szalay, P. G. with contributions from Auer, A. A.; Bartlett, R. J.; Benedikt, U.; Berger, C.; Bernholdt, D. E.; Bomble, Y. J.; et al. *CFOUR, Coupled-Cluster Techniques for Computational Chemistry*.
- (49) Raghavachari, K.; Trucks, G. W.; Pople, J. A.; Head-Gordon, M. A Fifth-Order Perturbation Comparison of Electron Correlation Theories. *Chem. Phys. Lett.* **1989**, *157*, 479–483.
- (50) Bartlett, R. J.; Watts, J. D.; Kucharski, S. A.; Noga, J. Non-Iterative Fifth-Order Triple and Quadruple Excitation Energy Corrections in Correlated Methods. *Chem. Phys. Lett.* **1990**, *165*, 513–522.
- (51) Stanton, J. F. Why CCSD(T) Works: A Different Perspective. *Chem. Phys. Lett.* **1997**, *281*, 130–134.
- (52) Dunning, T. H. Gaussian Basis Sets for Use in Correlated Molecular Calculations. I. The Atoms Boron through Neon and Hydrogen. *J. Chem. Phys.* **1989**, *90*, 1007.
- (53) Mills, I. M. Vibration-Rotation Structure in Asymmetric and Symmetric Top Molecules. In *Molecular Spectroscopy*; Rao, K. N., Mathews, C. W., Eds.; Academic Press Inc.: 111 5th avenue, New York 10003, 1972; Chapter 3.
- (54) Schneider, W.; Thiel, W. Anharmonic Force Fields from Analytic Second Derivatives: Method and Application to Methyl Bromide. *Chem. Phys. Lett.* **1989**, *157*, 367–373.
- (55) Stanton, J. F.; Lopreore, C. L.; Gauss, J. The Equilibrium Structure and Fundamental Vibrational Frequencies of Dioxirane. *J. Chem. Phys.* **1998**, *108*, 7190.
- (56) Stanton, J. F.; Gauss, J. Analytic Second Derivatives in High-Order Many-Body Perturbation and Coupled-Cluster Theories: Computational Considerations and Applications. *Int. Rev. Phys. Chem.* **2000**, *19*, 61–95.
- (57) Zalicki, P.; Zare, R. N. Cavity Ring-Down Spectroscopy for Quantitative Absorption Measurements. *J. Chem. Phys.* **1995**, *102*, 2708–2717.
- (58) Hodges, J. T.; Looney, J. P.; vanZee, R. D. Laser Bandwidth Effects in Quantitative Cavity Ring-down Spectroscopy. *Appl. Opt.* **1996**, *35*, 4112–4116.
- (59) Herzberg, G.; Spinks, J. W. T. In *Molecular Spectra and Molecular Structure: Diatomic Molecules*; Condon, U., Ed.; Prentice-Hall physics series; Van Nostrand: New York, 1950.
- (60) Titarchuk, T. A.; Halpern, J. B. Reactions of C₃N Radicals and HC₃N Metastables. *Abstr. Pap. Am. Chem. Soc.* **2000**, *220*, U212.
- (61) Luo, C.; Du, W.-N.; Duan, X.-M.; Li, Z.-S. A Theoretical Study of the Photodissociation Mechanism of Cyanoacetylene in its Lowest Singlet and Triplet Excited States. *Astrophys. J.* **2008**, *687*, 726–730.
- (62) Mbosei, L.; Fayt, A.; Drean, P.; Cosleou, J. Millimeter-Wave Spectra of HCCCN. *J. Mol. Struct.* **2000**, *517*, 271–299.
- (63) Hyde, G. E.; Hornig, D. F. The Measurement of Bond Moments and Derivatives in HCN and DCN from Infrared Intensities. *J. Chem. Phys.* **1952**, *20*, 647.
- (64) Kim, K.; King, W. T. Integrated Intensities in Hydrogen Cyanide. *J. Chem. Phys.* **1979**, *71*, 1967.
- (65) Smith, A. M. The Intensity and Self-Broadening of Overtone Transitions in HCN. *J. Chem. Phys.* **1986**, *85*, 4958.
- (66) Kim, K.; King, W. T. Integrated Infrared Intensities in HCCH, DCCD and HCCD. *J. Mol. Struct.* **1979**, *57*, 201–207.
- (67) Lehmann, K. K. The Absolute Intensity of Visible Overtone Bands of Acetylene. *J. Chem. Phys.* **1989**, *91*, 2759.